NOAA Technical Memorandum ERL PMEL-79

MODEL-DATA COMPARISONS FOR THE 1982-83 EL NIÑO: THE XBT TRACKS

D. E. Harrison

Pacific Marine Environmental Laboratory

William S. Kessler
Benjamin S. Giese

School of Oceanography
University of Washington
Seattle, Washington

Pacific Marine Environmental Laboratory
Seattle, Washington
May 1988

UNITED STATES DEPARTMENT OF COMMERCE

C.William Verity
Secretary

NATIONAL OCEANIC AND ATMOSPHERIC ADMINISTRATION

Environmental Research Laboratories

Vernon E. Derr,
Director

NOTICE

Mention of a commercial company or product does not constitute an endorsement by NOAA/ERL. Use of information from this publication concerning proprietary products or the tests of such products for publicity or advertising purposes is not authorized.

Contribution No. 1035 from NOAA/Pacific Marine Environmental Laboratory

For sale by the National Technical Information Service, 5285 Port Royal Road
Springfield, VA 22161

CONTENTS

MODEL-DATA COMPARISONS FOR THE 1982-83 EL NIÑO: THE XBT TRACKS

D.E. Harrison[1], William S. Kessler[2], and Benjamin S. Giese[2]

ABSTRACT. Five different analyses of 1982-83 monthly average surface wind stress fields have been used to force an ocean general circulation model of the tropical Pacific, in a series of El Niño hindcast experiments like that reported by Philander and Seigel (1985). The results of these hindcasts are compared here with the variability of upper ocean dynamic height, sea surface temperature and subsurface temperature as observed from XBT data obtained along the three main ship of opportunity tracks.

During 1982-83 there were prominent departures from climatology in the surface wind stress field. However, there are so few observations of surface wind available that efforts to produce fields of wind stress must fill in considerable gaps in data coverage, with the result that the various tropical surface analyses tend to differ considerably; the differences between analyses, along the ship tracks, are described. Generally the operational analyses produced by the meteorological centers (National Meteorological Center (NMC), European Center for Medium-range Weather Forecasting (ECMWF), and Fleet Numerical Ocean Central (FNOC)) had weaker surface stress and weaker spatial gradients than the special research products (Florida State University (FSU) and Sadler (SADLER)).

The ocean underwent several major changes during this period according to the XBT data; these changes are summarized. The model hindcasts are examined to determine the extent to which the observed major ocean changes were reproduced. Within the equatorial waveguide, dynamic height changes are hindcast with quantitative skill using each wind stress field; the best hindcasts differ from the observations by only a few dyn cm more than the estimated uncertainty in the observations. The large waveguide dynamic height hindcast skill found here indicates that the major elements of the 1982-83 El Niño are contained in the 1982-83 surface wind stress field, rather than in any particular aspect of the state of the ocean during late 1981. Sea surface temperature changes are generally hindcast with some qualitative skill; the correlation between hindcast and observed SST is usually significantly positive, but the RMS difference between any hindcast and the observations is generally greater than the RMS signal in the observations. Subsurface temperature variability is hindcast with differing levels of skill, depending upon stress field, region and depth. The vertical temperature gradients and mixed layer temperatures, as well as the depth of the thermocline, undergo substantial changes (especially in the eastern Pacific); primitive equation physics appear necessary to model these observations.

Outside the waveguide, hindcast skill is generally much reduced; although qualitatively correct behavior is often hindcast, amplitudes can be seriously in error. The most striking inconsistency found involves the NMC hindcast in the region of the North Equatorial Counter Current. The special research products generally give more accurate hindcasts of dynamic height, but the operational fields often produce better SST hindcasts. A clear deficiency of the operational fields is the character of their wind stress curl fields, compared either with climatology or the special research analyses; because Ekman pumping is a major factor in thermocline adjustment outside the waveguide, wind stress curl must be correctly represented if adequate hindcasts are to be obtained.

Although improved parameterization of upper ocean mixing, and better knowledge of the surface heat flux appear needed to improve SST hindcast skill, these results establish that a most serious need for improved hindcast performance is better knowledge of the surface wind stress field.

[1] NOAA/Pacific Marine Environmental Laboratory, 7600 Sand Point Way N.E., Seattle, WA 98115

[2] School of Oceanography, University of Washington, WB-10, Seattle, WA 98115

1. INTRODUCTION

The tropical Pacific warm event of 1982-83 was one of the strongest in the historical record, and followed a pattern of evolution quite different from that of the Rasmusson and Carpenter (1982) post-1950 composite El Niño-Southern Oscillation (ENSO) event. Although extremely anomalous conditions occurred in both the atmosphere and ocean and although these fluids were better observed than in any previous event, our understanding of the mechanisms responsible for the event remains very incomplete. The density of observations in space and time, while better than in any previous event, generally is not sufficient to permit direct diagnosis of these mechanisms. This is true particularly of the processes important for air-sea interaction in the coupled ocean-atmosphere system.

Although the ENSO phenomenon is fundamentally a feature of the coupled ocean-atmosphere system, much remains to be learned about the behavior of the individual fluids, treated as forced initial-boundary value problems, where the conditions at the air-sea interface are the forcing data. Because the air-sea forcing is known only subject to considerable uncertainty, an important aspect of any such "hindcasting" effort is to try to assess the impact of these uncertainties on the outcome of the hindcasts.

For ocean hindcasts one must have an approximation to the state of the ocean at the beginning of the hindcast period and must be able to impose or parameterize the surface fluxes of momentum, heat and liquid water over the period of interest. Recent efforts to estimate the uncertainty in monthly mean estimates of surface wind (e.g., Halpern and Harrison (1982), Luther and Harrison (1983), Harrison *et al.* (1984)) indicate that any two available analyses of the tropical Pacific will likely have RMS differences of roughly 2 m s^{-1}, in wind fields where the maximum speed is likely to be 79 m s^{-1} and the minimum wind may be near zero. Efforts to assess the likely uncertainty in monthly mean net surface heat flux suggest that the uncertainty will generally exceed 50 W m^{-2} (e.g., Niiler (1981)), in fields where typical climatological values range between zero and something over 100 W m^{-2}. Precipitation minus evaporation (the net liquid water flux) is generally neglected, because it is poorly known. Thus, from the outset there is concern that the forcing data will not be known as well as one would like it to be.

Philander and Seigel (1985) made a 1982-83 ocean ENSO hindcast, in which surface wind stress was estimated from National Meteorological Center (NMC) 1000 mb wind field analyses, surface heat flux was parameterized in terms of an imposed air-sea temperature difference and surface wind speed, and liquid water flux was neglected. This hindcast was able to reproduce some significant aspects of the 1982-83 event in the equatorial ocean, and has prompted efforts to develop a near real-time tropical Pacific ocean modeling activity at NMC. Their work also motivates the results described here.

Because the different monthly mean wind and pseudostress analyses differ so substantially from each other it is important to try to understand how these differences affect both our ability

to hindcast situations like the 1982-83 event, and to infer the dominant physical processes responsible for the changes that occurred during such events. Should certain aspects of the tropical Pacific upper ocean be determined largely by linear forced physics it should be straightforward to explain model hindcast differences in these quantities simply in terms of the differences in the stress fields. However, there is good reason to expect that many quantities, sea surface temperature (SST) and near surface currents in particular, will be determined by non-linear mechanisms (e.g., Schopf and Cane (1983), Schopf and Harrison (1983)), and hence *a priori* estimates of differences in these quantities are not likely to be simple to make.

We here report results from an effort to investigate the sensitivity of Philander and Seigel (1985) style hindcasts of the the 1982-83 ocean ENSO event to our uncertain knowledge of the monthly average wind stress field over the tropical Pacific. The reader is referred to Philander and Seigel (1985) for the background on their experiment and its physical motivation. The hindcasts reported here are carried out identically with the Philander and Seigel (1985) experiment, except that different surface wind stress analyses are used. For completeness and for comparison, the Philander and Seigel (1985) experiment was also repeated, and is designated NMC here.

The motivations for this work are several. First, as the TOGA and EPOCS programs are continuing to collect observations in the tropical Pacific, there is a need to assess our ability to do model hindcasts to investigate different aspects of the ocean's behavior. We must learn how well the surface wind field must be known in particular regions in order to obtain an adequate level of hindcast skill in experiments like these, and we must begin to assess what elements of hindcast error result from inadequacies in the model and its other parameterizations. A simple way to approach the first problem is to do hindcasts with the different available wind analyses, to evaluate the hindcast skill of each and to attempt to relate the differences to differences in the wind analyses. Secondly, through analysis of model hindcasts we can examine the mechanisms that may have been responsible for the changes that took place in the ocean during 1982-83. If similar mechanisms are found to be responsible for a particular sort of change in most of the hindcasts, and if the change had a clear correspondence with a change that occurred in the ocean, it is plausible to assume that these mechanisms were responsible for the behavior in the ocean. Thirdly, as mentioned above, there is a need to identify the elements which control the success of hindcasts such as these; linear equatorial theory indicates that a major factor should be the uncertainty in the wind stress forcing, but only through careful analysis of several hindcasts will it be possible to identify the other controlling factors needing study.

Three ship-of-opportunity XBT lines (see Section 2) provide for direct comparison of the model hindcasts with observed ocean variability. The variability of temperature and dynamic height calculated from XBT data is compared with that of the model hindcasts. In another work the hindcast SST and surface current results within the equatorial waveguide are of primary

interest. Section 2 provides a discussion of the changes observed from the XBT data along the tracks. Section 3 provides an overview of the different wind fields, how they were converted to stress fields for these hindcasts, the major changes observed in the fields, and statistics on the differences between the fields. Section 4 presents various timeseries from the data and the hindcasts, and highlights the role of Ekman pumping in controlling off-equatorial variability, while section 5 presents statistical hindcast results for 0/450 m dynamic height variation and for temperature variations at several depths. Section 6 offers some summary and discussion of hindcast findings, identifies a number of factors affecting hindcast skill, and offers some conclusions. Detailed comparison of the different wind analyses is presented in the Appendix.

2. EL NIÑO OBSERVED IN THE SHIP-OF-OPPORTUNITY XBT DATA SET

Expendable bathythermographs (XBTs) have been deployed since 1979 from merchant ships operating out of Noumea, New Caledonia under a joint U.S.-France ship of opportunity program. The same ships take bucket samples for the determination of surface temperature and salinity. The ships traverse nearly meridional routes in the central and western Pacific and an oblique route between Panama and Tahiti (Figure 1). The three routes will be referred to as the western Pacific (WP), central Pacific (CP) and eastern Pacific (EP) tracks, which cross the equator at 160°E, 165°W and 100°W respectively. A total of 5081 XBT profiles have been made on these routes during 1982-83, and these data form the basis for several studies of thermal variability in the tropical Pacific (Rebert *et al.* (1985); White *et al.* (1986); Kessler and Taft (1987). Kessler *et al.* (1985) evaluated the sensitivity of the estimation of various oceanographic quantities including dynamic height and geostrophic transport to varied XBT sampling situations in the CP. For the purpose of this study, any XBT profile taken within 10° longitude of the centerline of each track shown in Figure 1 was considered to lie on the track, and the longitudinal spread of the observations within each track was ignored. (The model hindcasts, on the other hand, were simply sampled exactly on the track centerlines). Approximately 2 profiles per degree latitude per month were made on each of the three ship routes during 1982-83, and the data were bin-averaged with a resolution of one degree latitude and one month. This averaging means that short-period fluctuations such as the 20/30-day waves in the eastern equatorial Pacific are poorly resolved and contribute to aliasing of the monthly data. Kessler and Taft (1987) discuss the gridding process and the errors inherent in the uneven sampling and non-meridional tracklines.

The three routes of the ship of opportunity program show three distinct thermal regimes during 1982-83. The observations are consistent with the eastward draining from the equatorial western Pacific of a pool of warm, relatively fresh water during the last half of 1982 and the appearance of this water in the central and eastern Pacific in September-October 1982 and January-March 1983 respectively. In the description which follows, we identify the few large-

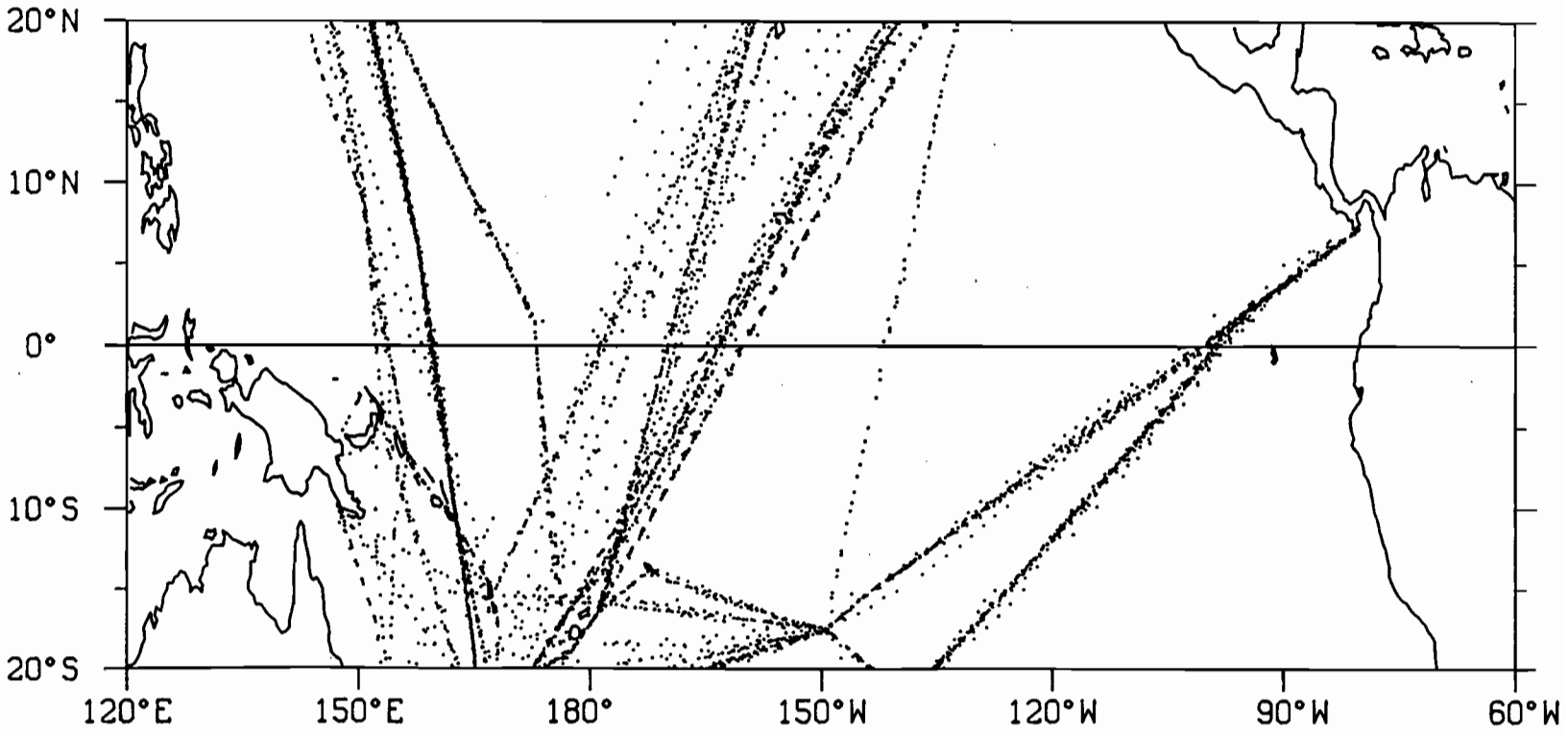

Figure 1: Geographical scatter of all XBT casts on the ship of opportunity XBT lines for the period 1982-83.

scale fluctuations which characterized the event in each region; the major events which any successful model hindcast must reproduce. Dynamic height, rather than the depth of a given isotherm, is shown because this integrated quantity includes the effects of both thermocline depth changes and mixed layer temperature and salinity changes. Dynamic height changes are generally found to be the inverse of thermocline depth fluctuations; the main exception (discussed below) involves the warm, fresh upper layer water which appeared in the central and eastern Pacific in late 1982-early 1983. Dynamic heights were calculated from the XBT temperature profiles and surface salinity observations according the method of Kessler and Taft (1987), which uses a mean T-S relation below the thermocline but models the mixed layer vertical salinity gradient (starting from the observed surface salinity) to be proportional to the temperature gradient. This method gives an estimate of dynamic height which agrees better with sea level variations measured at oceanic islands than the use of a mean T-S relation alone (Kessler and Taft, 1987). In the model hindcasts, on the other hand, the entire salinity field is known, so dynamic heights were calculated directly. Surface zonal geostrophic current speeds relative to 450 m are evaluated from the dynamic height gradient along the WP and CP tracks, and offer a useful perspective on the effects of the dynamic height changes. Geostrophic speeds along the EP track are not shown, because the flow normal to this sharply angled track is not useful in interpreting changes in the ocean.

The earliest clear change observable in the ship of opportunity data was a shoaling of the equatorial thermocline on the WP track. Figure 2 shows that equatorial dynamic height on the WP track fell 8 dyn cm between February and April 1982. The shoaling extended from 2°S to 7°N in early 1982; it would ultimately extend from 15°S to 15°N by the end of the year. After a brief rise in July 1982 WP equatorial dynamic height fell 30 dyn cm in six months (Figure 2). This change was due to a 60 m rise in the thermocline which nearly eliminated the usual 100 m thick upper layer. Despite the large anomalies in the thermocline, SST changes were modest; WP equatorial SST fell about 1°C in mid-1982, to about 29°C, and remained at this level for about a year (Figure 3). Surface salinity changed much more than SST, climbing about 0.8‰ between July 1982 and April 1983 (Figure 4). In January 1983 WP equatorial dynamic height reached its nadir, and through 1983 dynamic height recovered slowly to about 10 dyn cm below its level at the beginning of 1982 (Figure 2).

On the CP track, equatorial SST gradually warmed more than 2°C during March to July 1982 and remained near 29°C for a year (Figure 3). CP equatorial surface salinity was normal until July 1982 and then rapidly began falling; the total decrease of 1‰ by October was to a level typical of pre-Niño conditions in the WP (Figure 4). Extreme rainfall occurred in the CP, however the peak precipitation occurred in December 1982-January 1983, which lagged the lowest salinity by 2 months. Kessler and Taft (1987) concluded that both advection from the west and local rainfall contributed to the low surface salinity in the equatorial CP.

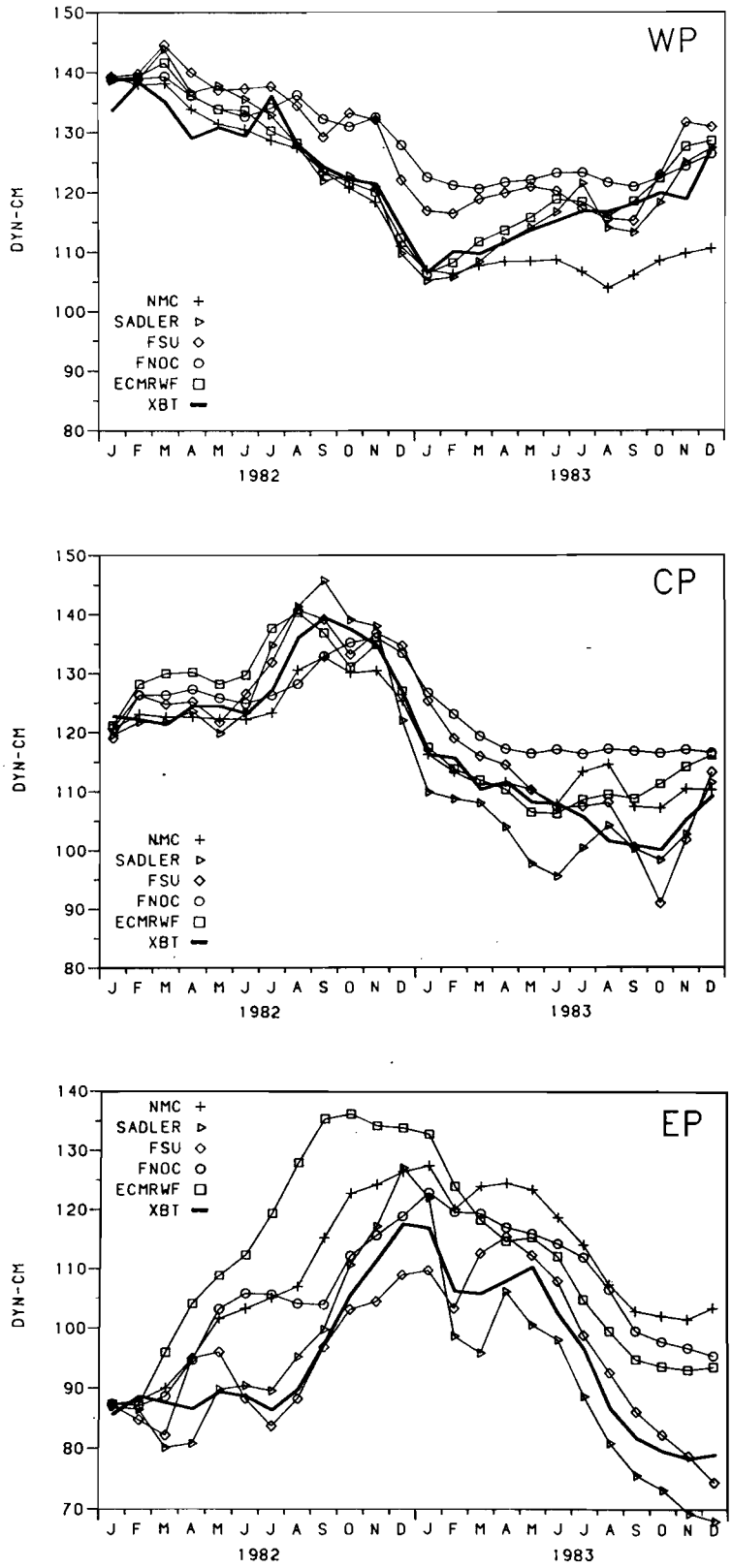

Figure 2: Dynamic height at the equator on the three ship tracks from the XBT data and model hindcasts. Top panel: western Pacific; middle panel: central Pacific; bottom panel: eastern Pacific.

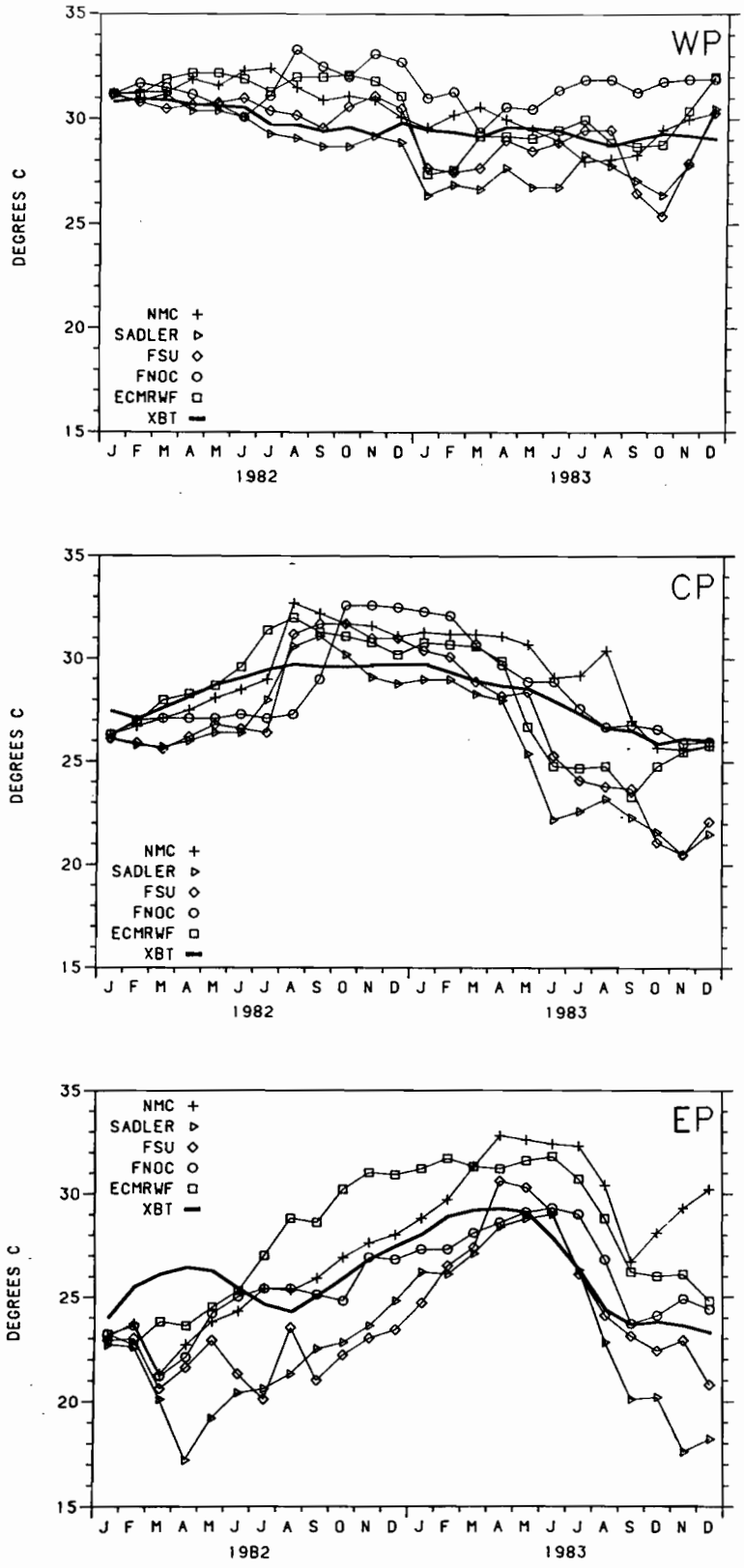

Figure 3: Sea surface temperature at the equator on the three ship tracks from the XBT data and model hindcasts. Top panel: western Pacific; middle panel: central Pacific; bottom panel: eastern Pacific.

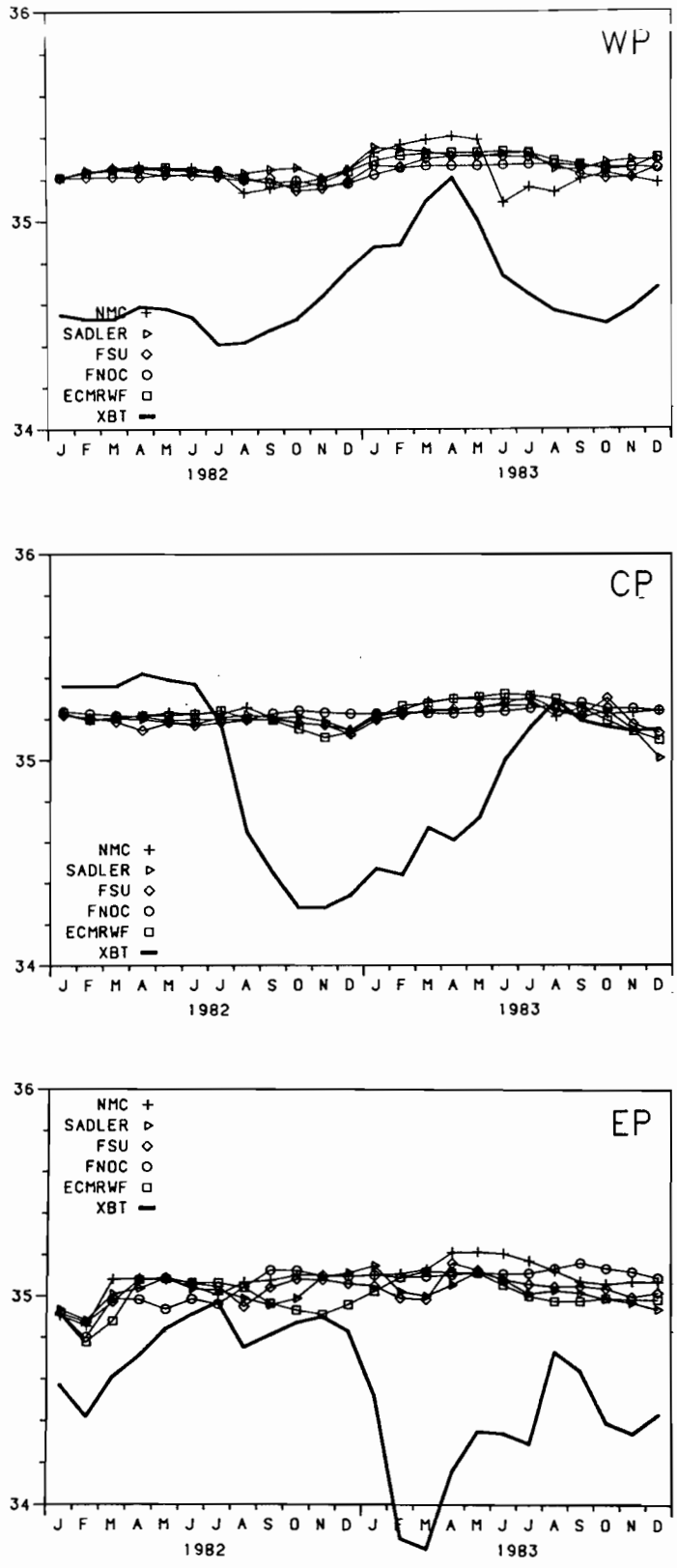

Figure 4: Sea surface salinity (parts per thousand) at the equator on the three ship tracks from the ship of opportunity data and model hindcasts. Top panel: western Pacific; middle panel: central Pacific; bottom panel: eastern Pacific.

CP thermocline changes did not occur until July-August 1982, when the thermocline deepened by about 20 m to more than 100 m deep and the vertical gradient between 28° and 18°C became very sharp. The upper layer was then deeper than it had been at any time in the previous 3 years (Kessler and Taft, 1987). The 15 dyn cm rise in CP equatorial dynamic height between July and September 1982 (Figure 2) was largely due to the thick, very low-density upper layer (about half the rise was due to the low salinity alone (Kessler and Taft, 1987)).

At the end of 1982 equatorial CP dynamic height fell precipitously, dropping 20 dyn cm during December 1982 and January 1983 (Figure 2). This was due to a rapid 50 m rise in the thermocline; changes in the CP thermocline at the end of 1982 resembled those which had occurred several months earlier in the WP. Unlike the WP, however, dynamic height in the CP continued to drop until October 1983, falling an additional 15 dyn cm (Figure 2); much of the change after the initial large thermocline rise was due to cooling of the upper layer. During most of 1983 CP SST fell slowly to below 26°C (Figure 3), which was lower than observed on this track at any time in the preceding seven years (Kessler and Taft, 1987). During the first half of 1983 the surface salinity returned to normal (Figure 4). These changes occurred simultaneously with strong westward geostrophic flow spanning the equator during 1983 (see discussion below).

In the eastern Pacific conditions were normal until August 1982, when the equatorial thermocline began dropping and deepened steadily until the end of 1982, by which time the 20°C isotherm was about 80 m deeper and the thermocline sharper than it had been during the previous year (Figure 5, upper left). At the same time the SST climbed steadily; however the upper layer temperature did not reach its peak until April 1983 (Figure 3). By January 1983 dynamic height on the EP track had risen 30 dyn cm. At that time it was higher in the EP than in the WP and equal to that in the CP; there was approximately zero pressure gradient across the Pacific basin (Figure 2). The warming surface layer accounted for about one-third of the dynamic height rise. In February and March 1983 EP equatorial dynamic height fell 12 dyn cm as the thermocline recovered partly back to normal levels and more typical vertical gradient (Figure 5); in April dynamic height climbed again to a second peak (Figure 2). This second peak was not reflected in changes in the sharpest region of the thermocline (for example 20°C is nearly flat at this time), but depth changes in isotherms below 20°C were almost as large as those which took place during the first drop in late 1982 (Figure 5); this had the effect of spreading the lower thermocline and reducing the stratification. The 12°C isotherm remained at approximately constant depth at this time, so the deepening of the lower thermocline meant that the usually thick thermostad region of 13°C water contracted to about one-third its normal depth extent (Figure 5). Clearly the dramatic changes in stratification that occurred within the main thermocline, above it in the surface layer and below it in the thermostad, cannot be described by a few vertical modes.

During June-November 1983 dynamic height on the EP track fell as the thermocline rose and the warm upper layer disappeared (Figure 5). In October 1983 dynamic height on all three

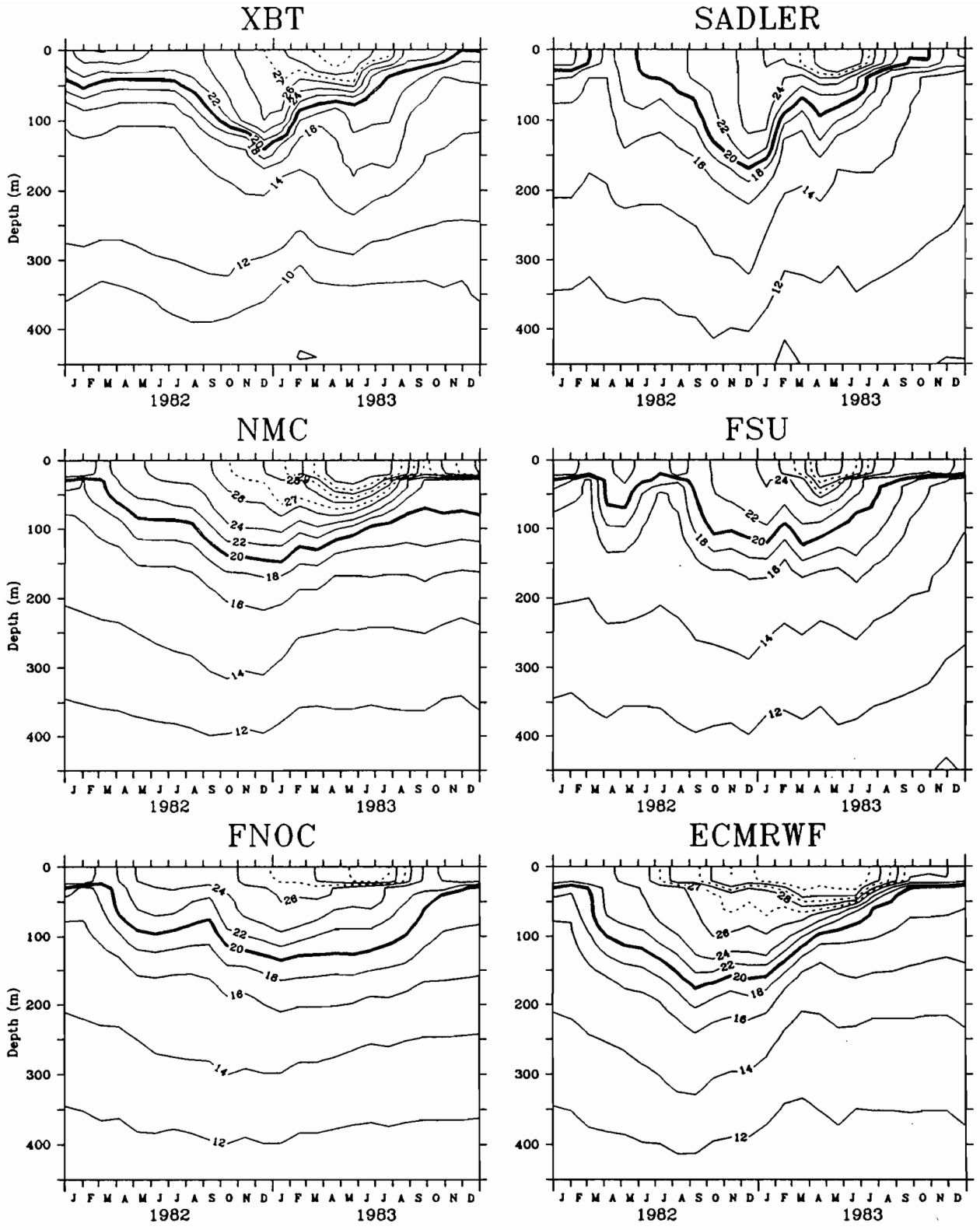

Figure 5. Temperature at the equator on the eastern Pacific track from the XBT data and model hindcasts.

tracks was 10 to 20 dyn cm lower than it had been in January 1982 (Figure 2). Wyrtki (1984) noted that sea level measured at equatorial island stations was similarly low in October 1982 and concluded that this was the result of a draining of warm water out of the equatorial Pacific during El Niño.

Changes in the thermal structure away from the equator were equally as dramatic as those at the equator, and were associated with large variations in the transport of the major zonal geostrophic currents. On the WP track, dynamic height at 10°N fell 33 dyn cm between April and November 1982 (Figure 6). This change, which was larger and peaked earlier than the dynamic height fall on the equator, was due to a 60 m shoaling of the thermocline. It had the effect of increasing the pressure gradient across the eastward North Equatorial Countercurrent (NECC), and WP NECC geostrophic transport jumped to 34 Sv (1 Sv = $10^6 m^3 s^{-1}$) in October 1982 (the 1979-81 mean had been about 24 Sv). The reader is referred to Kessler and Taft (1987) for a discussion of the estimation of geostrophic transport from the XBT data.

On the CP track, thermocline shoaling also occurred at 10°N in mid and late 1982, although not quite as strongly as in the WP (Figure 6). The shoaling was in phase with the usual seasonal shoaling in the CP, and appeared as an exaggeration of the seasonal cycle (Kessler and Taft, 1987). The combination of the shallow thermocline ridge near 10°N and the deep warm fresh equatorial upper layer increased the pressure gradient across the CP NECC, and NECC transport doubled to 42 Sv in November 1982, with surface speeds about 80 cm s^{-1} at 5°N (Figure 7, upper left).

The warm equatorial upper layer in the CP in late 1982 also eliminated the usual equatorial trough in dynamic height which is associated with the westward South Equatorial Current (SEC) spanning the equator (Figure 7, upper left). No attempt is made to calculate geostrophic currents closer to the equator than 2° latitude, but direct current measurements at 159°W show that the equatorial undercurrent was very weak from September to December 1982 and that an eastward equatorial surface jet with speeds up to 140 cm s^{-1} occurred in October to December 1982, replacing the SEC at the equator with eastward flow (Firing *et al.*, 1983). During the Hawaii-Tahiti Shuttle (197980) average net zonal volume transport between 10°N and 10°S was approximately zero (42 Sv westward in the SEC, 23 Sv eastward in the EUC and 20 Sv eastward in the NECC (Wyrtki and Kilonsky, 1984)). In contrast, during November 1982 the SEC was reduced to a small remnant south of 5°S (Figure 7) with westward transport of 12 Sv, the EUC was nearly absent, NECC transport was 42 Sv eastward and the equatorial jet observed by Firing *et al.* (1983) transported at least 30 Sv eastward, for a net transport in the same region of more than 60 Sv eastward (Kessler and Taft, 1987).

While in 1982 major anomalies were observed on and north of the equator on the CP and WP tracks, during 1983 the largest changes were south of the equator. Along each track the thermocline shoaled more than 60 m between October 1982 and May 1983 from the equator to

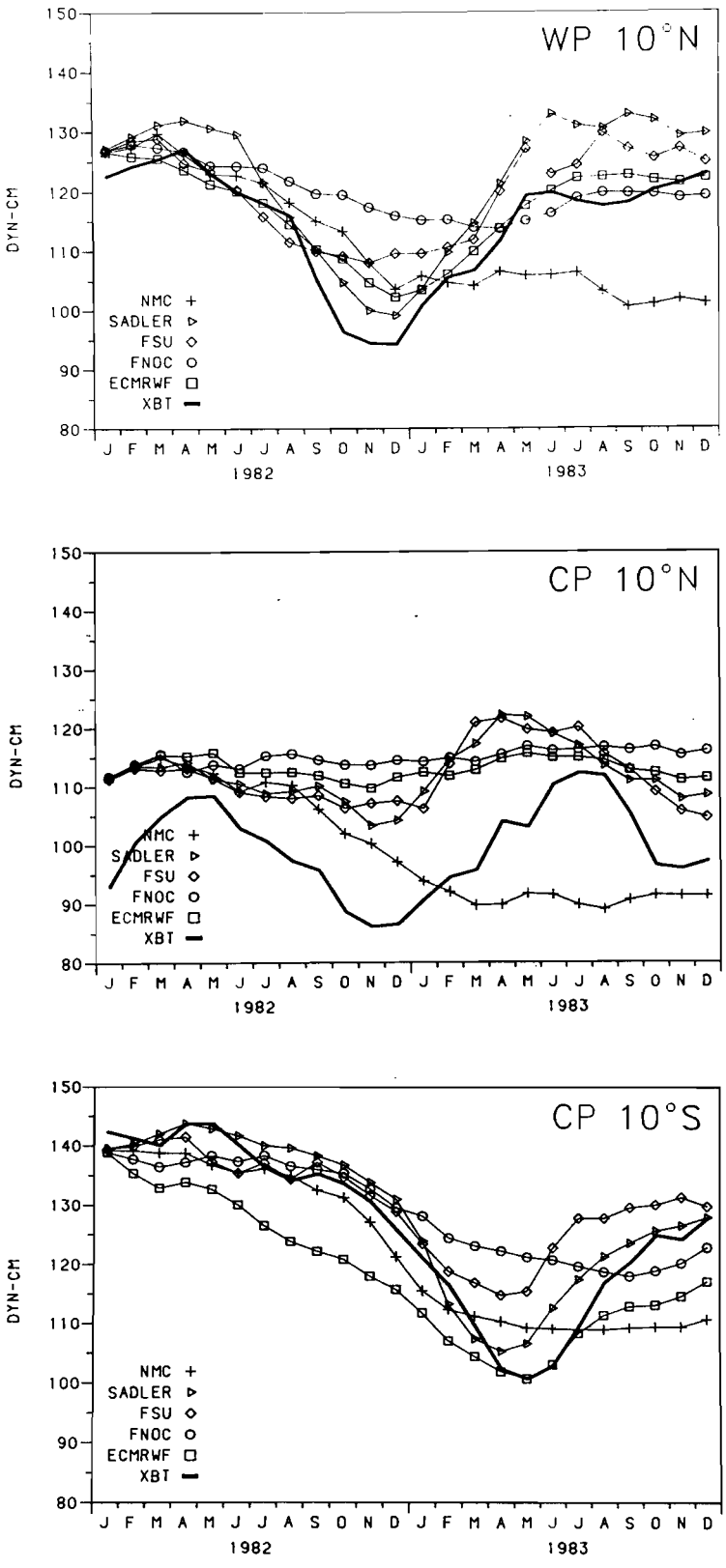

Figure 6. Dynamic height from the XBT data and model hindcasts. Top panel: 10°N on the western Pacific track; middle panel: 10°N on the central Pacific track; bottom panel: 10°S on the central Pacific track.

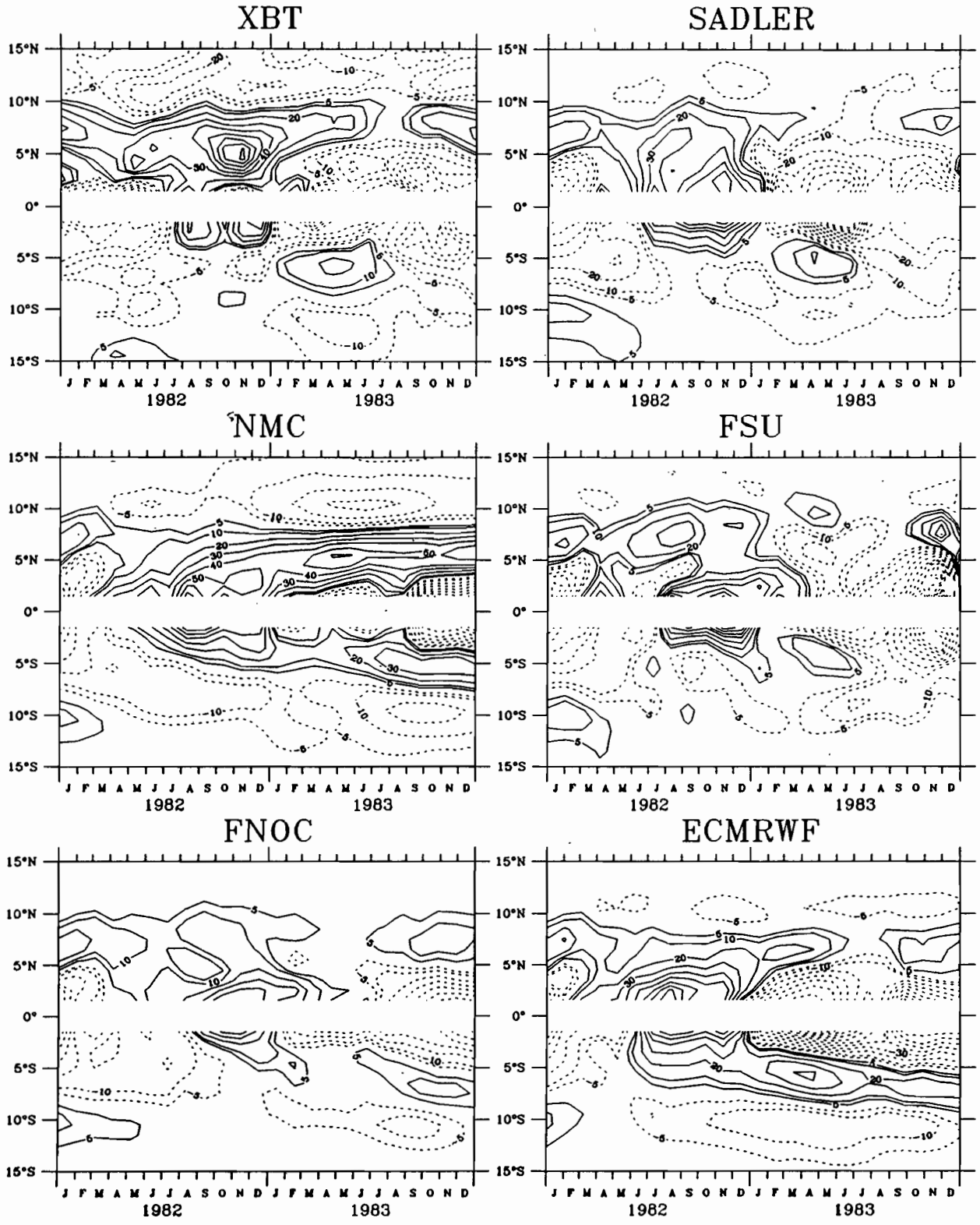

Figure 7. Surface zonal geostrophic speed (cm s^{-1}) relative to 450 m on the central Pacific track from the XBT data and model hindcasts.

12°S, causing a dynamic height drop of more than 40 dyn cm at 10°S in the CP (Figure 6). Wyrtki (1984b) noted that sea level at Funafuti Island (9°S, 179°E) dropped 40 cm below normal by June 1983, which is consistent with the dynamic heights estimated here. Kessler and Taft (1987) showed that this extreme anomaly (larger than any other dynamic height fluctuation in these data) was likely due to Ekman upwelling on the south flank of a belt of strong (7 m s^{-1}) westerlies centered near 5°S in the CP in the early months of 1983 (see Section 3). Wyrtki (1984b) interpreted the changes in sea level as a southward displacement of the southern subtropical gyre. The downward slope of the thermocline which ordinarily characterizes the region between 5° and 15°S was now found at 10° to 20°S, and this slope was associated with a fairly weak SEC (speeds about 15 cm s^{-1}); in this region there is usually near-zero or weak eastward flow (Figure 7).

The shoaling of the thermocline in the southern hemisphere occurred nearly simultaneously with the equatorial shoaling, resulting in an uplifted thermocline and low dynamic heights stretching across the equator from 5°N to 12°S in both regions during mid-1983. At 10°N dynamic heights rose in mid-year in accordance with the usual annual cycle (Kessler and Taft, 1987), and the combination of the seasonally high 10°N dynamic height and the abnormally low equatorial dynamic height nearly eliminated the pressure gradient across the NECC, and NECC transport fell below 5 Sv in July 1983 on both the CP and WP sections (Figure 7).

3. THE WIND STRESS FIELDS

The momentum flux (wind stress) at the ocean surface must be specified for the hindcasts to be carried out; a number of different analyses are available for 1982-83. Three sets of monthly mean surface stress fields were produced from operational meteorological center products: by N. Wells (personal communication, 1985), using data from the European Center for Medium Range Weather Forecasting (ECMWF), by Philander and Seigel (1985) using the 1000 mb winds from the National Meteorological Center (NMC) and by us, using six-hourly nominal 10-m height winds from the Fleet Numerical Ocean Central (FNOC) (their A-29 and A-30 surface marine wind products). Monthly mean pseudo-stress analyses were produced by Florida State University (FSU) from surface data (Goldenberg and O'Brien, 1981) and by J. Sadler (SADLER) from low-level cloud motion vectors, a climatological wind shear field between the surface and cloud level, and surface observations (Sadler and Kilonsky, 1985). The pseudostress fields must be multiplied by air density times drag coefficient (C_d) to obtain stress values.

The FNOC wind data were converted to stress fields using the C_d formulation of Large and Pond (1981) and assuming relative humidity of 0.75 and climatological air-sea temperature differences; these stresses were then monthly averaged. Two FSU stress fields were made from the FSU pseudostress fields – using $C_d = 1.2 \times 10^{-3}$ and $C_d = 1.5 \times 10^{-3}$ – for separate experiments. 1.2×10^{-3} is a reasonable value for winds of roughly 5 m s^{-1} under typical central tropical

Pacific conditions according to Large and Pond (1981), while 1.5×10^{-3} is the value used by Wyrtki and Meyers (1975) and is typical of the Bunker (1976) C_d formulation for these conditions. In most respects the weaker stress field gave better results than the stronger field; results denoted FSU pertain to the weaker stress fields. The Sadler (SADLER) stress fields were made from the Sadler pseudostress fields using $C_d = 1.2 \times 10^{-3}$.

These fields provide the forcing data for the hindcasts to be discussed here. Although a detailed discussion of the differences between the different stress fields will not be offered, it is useful to consider certain common elements of the fields and the major differences between them. Before examining specifics along the different ship tracks, some general comparisons can be offered. Overall there is considerable qualitative similarity between the different stress fields. The FSU and SADLER fields are generally the most similar, not surprisingly as they both depend heavily upon ship wind observations, but the FSU fields generally possess more spatial variability in a given month and greater month to month variability in a given location. FSU amplitudes are typically 20% smaller than SADLER amplitudes, although the same drag coefficient was used in each case. Although FNOC also makes heavy use of ship observations, the results of the stress calculation here produced fields both much weaker in amplitude than FSU and sometimes quite different in spatial structure from FSU and SADLER. The ECMRWF and NMC fields tend to exhibit the least spatial structure, not surprisingly as they are produced on grids with the coarsest meridional resolution of any of the fields.

Figure 8 shows the vector stress timeseries according to SADLER, and serves to illustrate the major wind changes that took place during 1982-83. We show the SADLER fields because the changes are large enough to be seen easily, because there is often qualitative similarity to the other fields, and because good hindcast results for dynamic height variability are frequently obtained with the SADLER fields. The Hellerman and Rosenstein (1983) climatological stress fields are also shown in Figure 8 for reference.

In the western Pacific (Figure 8, top panels) the normal regime prevailed early in 1982, with the (boreal) winter monsoon pattern in evidence; the austral summer northwesterly monsoon between 5° and 15°S was stronger than climatology in January 1982. In March 1982 there was westerly stress on and just south of the equator, when climatologically the western Pacific easterlies are at their seasonal maximum. The usual southern hemisphere SE trades began to build in May 1982, but unusually intense southerly flow appeared in the southern hemisphere in June/July, while westerly stress extended from about 2°S to as far as 10°N (Harrison, 1984). The anomalous westerly flows continued for at least several months. The NE Trades returned abruptly in December 1982, and brought unusually strong northerly cross-equatorial flow that persisted for several months; during the first months of 1983 there was also strong westerly stress between about 5° and 12°S. The SE Trades re-formed in mid-1983, with somewhat greater than usual strength near 5°S.

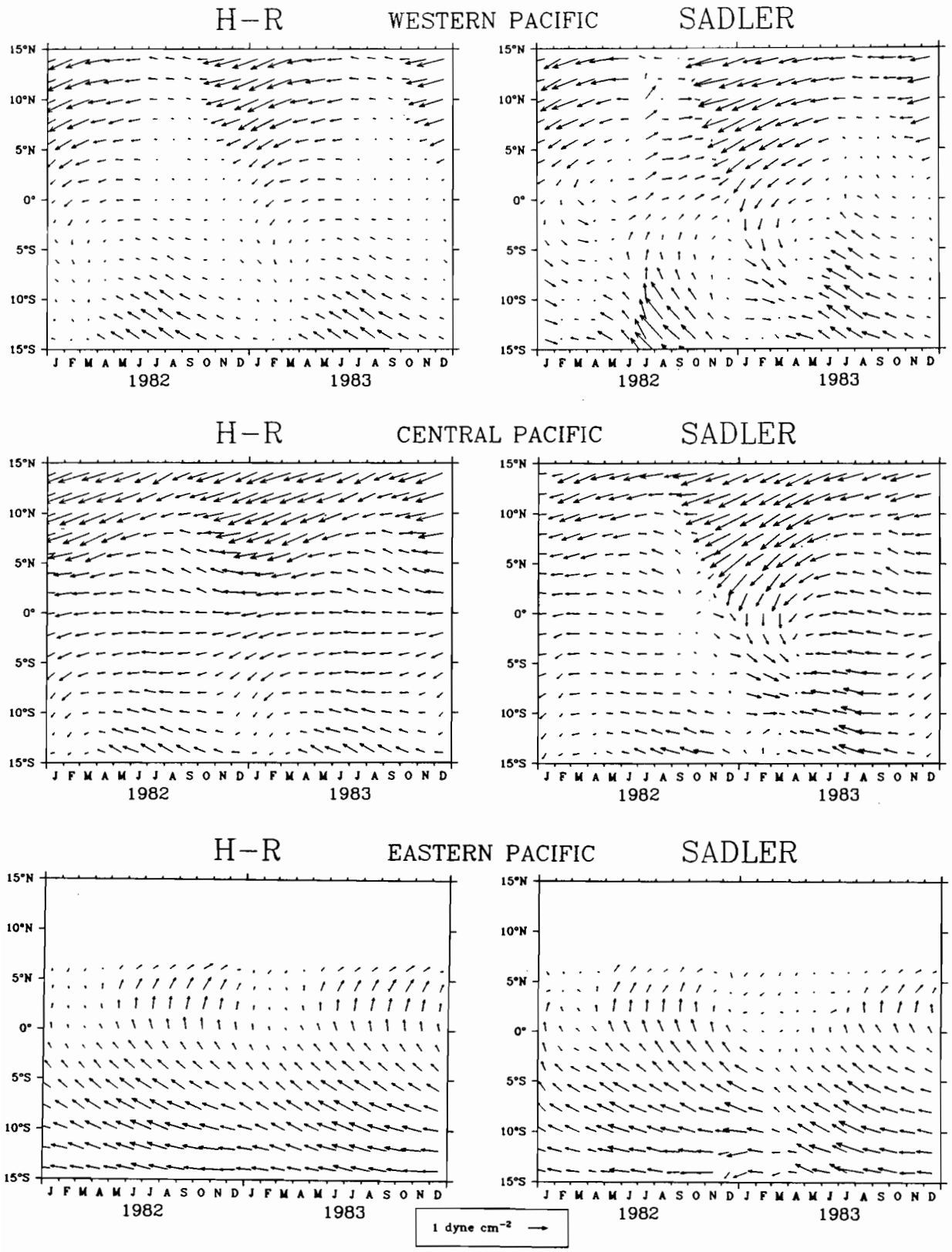

Figure 8. Monthly mean surface wind stress vectors on the three ship tracks from the Hellerman and Rosenstein (1983) climatology and the Sadler wind analysis. Left panels: Hellerman and Rosenstein; right panels: Sadler. Top panels: western Pacific; middle panels: central Pacific; bottom panels: eastern Pacific. The scale vector at bottom center indicates 1 dyne cm^{-2}.

Along the central Pacific track (Figure 8, middle panels) the prevailing trade wind regime was less visibly disrupted, except between September 1982 and April 1983. The usual waveguide easterlies were replaced by calm conditions in September 1982. Weak westerly stress began on and just north of the equator in October. In November westerly stress reached 0.4 dyne cm^{-2} centered on the equator; thereafter westerlies were only found south of the equator. Between January and March 1983, winds were similar to those seen on the western track, with northerlies extending across the equator and westerlies between 5° and 10°S; of course these represent much larger anomalies than in the WP. Normal conditions returned by May 1983 on the equator. The core of the SE trades (roughly 10°S) was stronger than usual in June-July 1983.

Along the eastern Pacific track (Figure 8, lower panels) the departures from climatology tended to be isolated to a few particular months of weaker or stronger than normal prevailing conditions. The only clear period of unusual conditions was March-April 1983, when the winds tended to be unusually light.

Those interested in the how the different wind fields compare in detail should consult the Appendix, which presents a variety of figures describing the different wind fields and their statistics. For a quick look, Figure 9 shows the different zonal wind stress fields along the equator for the three tracks, with the Hellerman and Rosenstein (1983) climatology for comparison. Many qualitative similarities exist between the analyses: predominantly westerly stress from July through November 1982, followed by an abrupt return to easterly stress in December 1982 in the WP, predominantly westerly stress in October-December 1982, followed by a return to easterly stress in January 1983 in the CP, and very small stress in May-June 1983 in EP. But there are also qualitative differences of note: the early occurrence of westerlies in 1982 in the CP (ECMRWF) compared to the others, the sharp drop in easterly stress in the CP in October 1982 in SADLER, FSU and FNOC compared to a small decrease (NMC) or (oppositely) a reduction in westerly stress (ECMRWF), the very weak stress that persists through the middle of 1983 in NMC and FNOC compared with the return of substantial easterlies in the others, etc. The Appendix statistics reveal that differences of 0.2-0.3 dyne cm^{-2} are common, and that differences of 0.5 dyne cm^{-2} are not unusual.

Overall, the quantitative comparisons indicate that our knowledge of the monthly surface stress variations in the tropical Pacific, at least as measured by the typical differences between products, remains uncomfortably large. There is quite good agreement on the gross character of the changes during the 82-83 event, but quantitative agreement remains elusive even at the level of 0.2 to 0.3 dyne cm^{-2}.

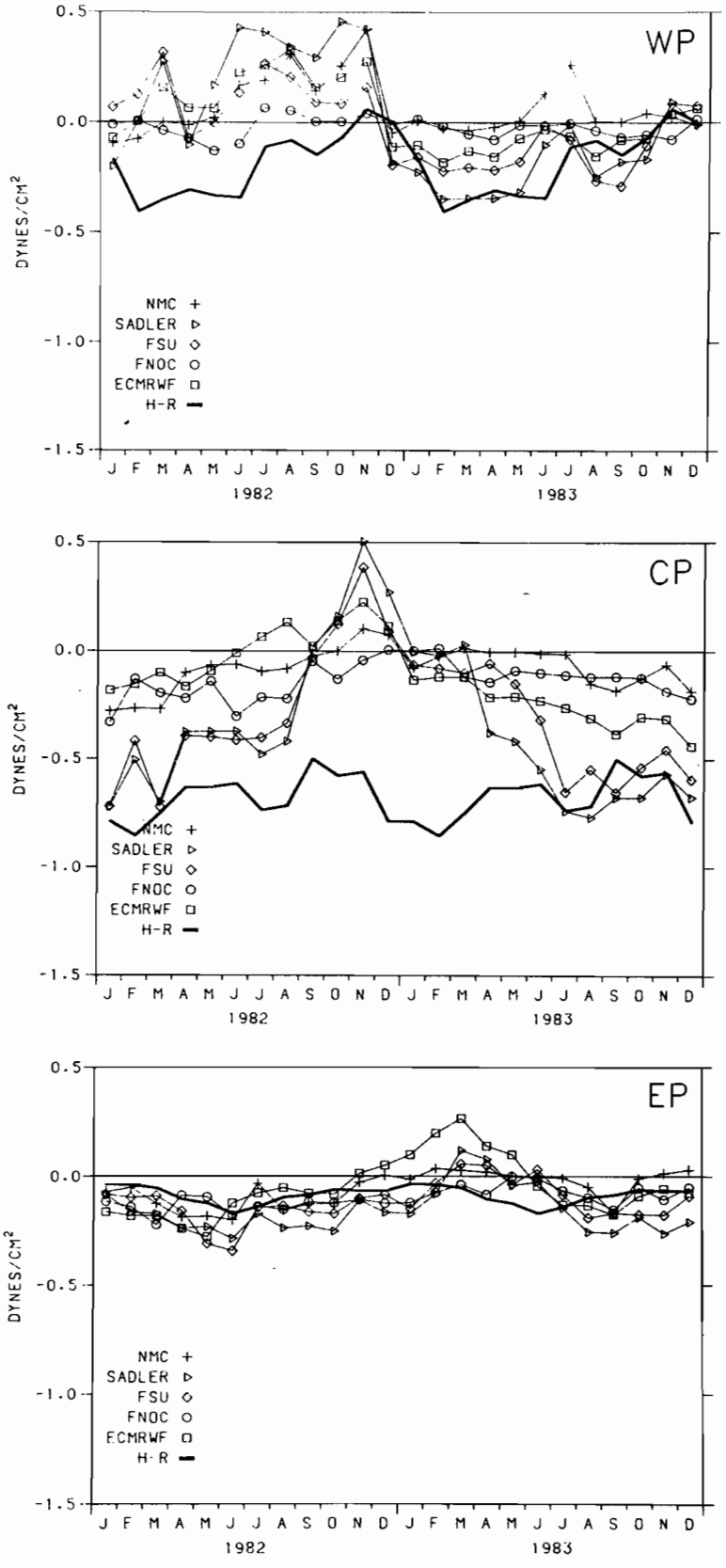

Figure 9: Zonal component of the wind stress (τ^x) at the equator on the three ship tracks from the Hellerman and Rosenstein (1983) climatology and the five wind products studied. Top panel: western Pacific; middle panel: central Pacific; bottom panel: eastern Pacific.

4. EL NIÑO OBSERVED IN THE MODEL RUNS

In this section timeseries of dynamic height, zonal geostrophic speed and surface temperature and salinity are used to compare specific features of the model response to each of the five wind sets. A detailed discussion of hindcast statistics is postponed to Section 5.

4.1 Common features

The model runs as a group did reasonably well in hindcasting many of the large-scale features of the El Niño within 2 or 3 degrees of the equator, in particular the dynamic height field. Correlation of near-equatorial 0/450 m dynamic height (Figure 2 and Section 5) of all the models with the XBT observations was above .9 on the WP and CP tracks and above .8 on the EP track. All the hindcasts showed the year-long fall of equatorial dynamic height in the WP during 1982 (Figure 2). In the CP, all the runs reproduced an upward peak of equatorial dynamic height and SST in late 1982 and the sharp fall during 1983 as observed (Figure 2). Associated with these dynamic height events spanning the equator were large changes in the zonal geostrophic currents (Figure 7), which were found by differencing the dynamic height fields in the regions poleward of 2° latitude. In both the CP and WP, the hindcasts all showed an increase in eastward geostrophic flow north and south of the equator in late 1982 which was similar to observations. In 1983 in the CP, all the runs reproduced the strong westward SEC spanning the equator, and all except the NMC run showed the near-disappearance of the NECC in mid-1983, with westward flow extending to 6°-7°N as observed. In the EP, dynamic heights on the equator were more scattered about the data than on the other two tracks, but the phases of the fluctuations were quite similar for most of the runs (Figure 2). The double peak of dynamic height was evident to some degree in all but one case (ECMRWF), however the vertical structure of these peaks was usually not well reproduced (Figure 5).

Some discrepancies with the observations common to all the model runs are due to model ocean conditions at the beginning of the hindcast in January 1982. The initial condition for all the hindcasts is constructed by initialization with the Levitus climatological temperature and salinity (Levitus, 1985), followed by two years of spinup with seasonal winds (Philander and Seigel, 1985). Figures 2 through 7 show that the hindcasts for all variables were nearly identical in January 1982, which uses values sampled at day 17 of the hindcast integration. Zonal geostrophic speeds (Figure 7) demonstrate some differences between the model and observed ocean at the beginning of the hindcast. In January 1982 the model North Equatorial Current (NEC) was only about one-quarter as strong as observed. Since the climatological initialization (Levitus, 1985) depicts the NEC to be about as strong as observed in the XBT data, this weakening must have been due to processes operating during the two-year spinup. At the end of the spinup period a relatively strong South Equatorial Countercurrent (SECC) (about 10 cm s^{-1}) was found near 10°S in the WP and CP, which is in accord with observations of a normal year in the

XBT data, but was not the case at the beginning of 1982 in the CP (Kessler and Taft, 1987). On the other hand, the model NECC at the end of the spinup was only slightly weaker than observed in the XBT data in January 1982 on the CP track.

Surface temperature and salinity were in general poorly hindcast by all of the model runs. Hindcast SST variability was considerably larger in almost every location than observed variability (see Section 5), and the model developed unrealistically high surface temperatures during the peak of the El Niño in several of the runs (Figure 3). Evaporative heat loss is an important contribution to the air-sea heat flux in the model (Philander *et al.*, 1987), and the two wind sets with the weakest wind speeds (FNOC and ECMRWF) generally developed the highest SST, while the two sets with the highest speeds (SADLER and FSU) had the lowest SST. Surface salinity fluctuations in the model, in contrast, were about an order of magnitude smaller than those observed (Figure 4). The observed salinity variations were an important contribution to the XBT dynamic height changes, particularly in the CP where low salinity accounted for about half the 15 dyn cm peak in late 1982 (see Section 2), so a successful hindcast requires a realistic salinity field. In this case the error in hindcast dynamic height in the CP was reduced since the overestimation of high SST tended to compensate for the underestimation of low salinity (Figure 3). The model does not have any fresh water input, so the hindcasts had no forcing similar to the extreme rainfall observed in the CP in late 1982. In addition, the hindcast period began with very weak zonal salinity gradients compared to the ocean (Figure 4), so anomalous zonal advection of salt, which has been suggested as a mechanism for the large fluctuations observed in the CP (Kessler and Taft, 1987), could not occur in the hindcasts. The Levitus climatology of surface salinity is similar to that observed by the ship-of-opportunity program, thus the differences seen at the beginning of the hindcast period are due to the two years of model spinup. The lack of horizontal surface salinity gradients anywhere in the model ocean suggest that with no atmospheric forcing the model upper layer salinity is simply well-mixed.

In this section we also examine the extent to which Ekman pumping accounts for the extra-equatorial differences noted between the various model runs. The Ekman pumping balance is written:

$$-\partial h/\partial t = \mathrm{curl}_z(\tau/\rho f),$$

where h is the depth of the 20°C isotherm (positive down), τ the wind stress, ρ the density of seawater and f the Coriolis parameter. Previous studies (Meyers, 1979, Kessler and Taft, 1987), studying the FSU and Sadler wind products respectively, showed that the annual variance in 20°C depth is in phase with the local wind stress curl and that Ekman pumping accounts for 50% or more of the annual variance of 20°C depth in some areas, particularly near 10°N and poleward of 10°S in the CP. By controlling thermocline depth fluctuations in these regions, the local wind stress curl determines much of the seasonal variability of the two tropical countercurrents, the

NECC and SECC. In addition, the large southern hemisphere thermocline shoaling observed in early 1983 (see Section 2) was shown to be the result of strong cyclonic curl associated with the westerlies centered near 5°-10°S in the CP (Figure 8) (Kessler and Taft, 1987). It is reasonable to examine whether this mechanism accounts for a high proportion of model variance as well. Figure 10 summarizes the correlation of the vertical motion of the depth of the 20°C isotherm in each model run with the curl of the corresponding local wind stress. Specific cases are discussed in the sections on each model run below. We note that although in the CP and WP many instances are observed of the model variance dominated by Ekman pumping, in the EP there is at best marginal correlation significance for any of the runs (Figure 10).

4.2 NMC

The NMC hindcast, which has previously been discussed by Philander and Seigel (1985), is in most respects the least like the XBT observations of any of the model runs.

In the WP on the equator, NMC dynamic height fell similarly to the observations during 1982, but never recovered during 1983, so by the end of the hindcast period NMC dynamic heights were about 15 dyn cm lower than those observed in the XBT data and all the other model runs (Figure 2). On the EP track, on the other hand, NMC dynamic height ended the hindcast period with equatorial dynamic height about 25 dyn cm higher than observed (Figure 2). Thus the zonal dynamic height difference across the basin at the end of 1983 was only 6 dyn cm in the NMC hindcast, compared to 48 dyn cm in the XBT data and similar amounts in the other model runs. NMC wind stress on the equator never rose much above 0.2 dyne cm^{-2} anywhere and averaged near zero on all three tracks, compared to the seasonal winds which averaged 0.6 dyne cm^{-2} in the CP (see Section 3). We might interpret the NMC equatorial hindcast as the response of the model ocean steadily adjusting to a diminishing and then very weak easterly stress field.

The hindcast vertical profile of equatorial temperature on the EP track (Figure 5) was similar to the XBT profile during 1982, but had a different character during 1983. While the observations show a distinct downwelling event in the lower thermocline during February to June 1983, the NMC hindcast shows a steady upward trend. The second peak in dynamic height in the NMC EP hindcast (Figure 2) is due primarily to the very high upper layer temperature (SST greater than 32°C), and not to thermocline variations as in the XBT observations.

The hindcast NECC in the CP and WP strengthened in late 1982 as in the observations, but then continued to strengthen during 1983 while the observed NECC (and the NECC in all the other runs) nearly disappeared (Figure 7). At 10°N in the CP and WP (near the northern boundary of the NECC), the model hindcast a fall in dynamic height during late 1982 resembling the observations, but unlike the observations, NMC dynamic heights never recovered from the drop and remained about 20 dyn cm below those observed (Figure 6); consequently a large pressure

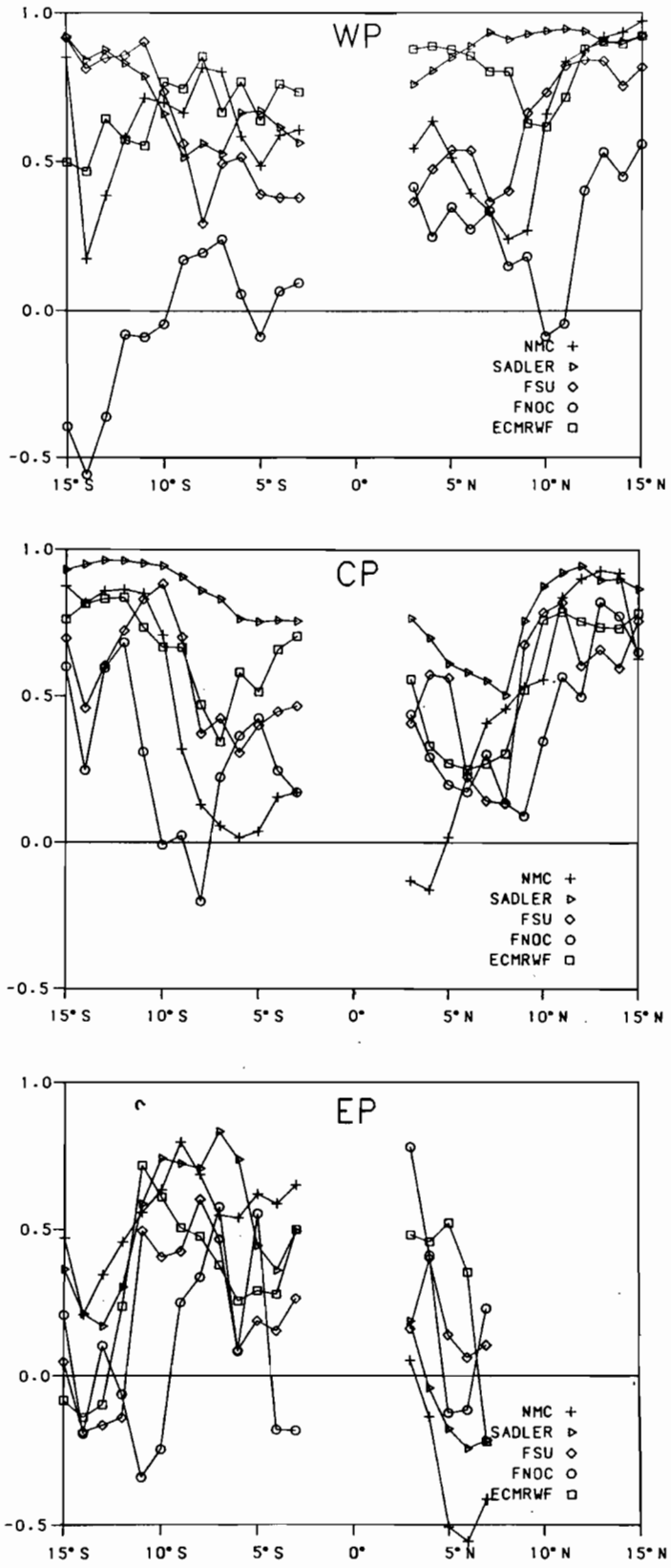

Figure 10: Correlation of the Ekman pumping balance on the three ship tracks from the five model hindcasts. In each case $\partial h/\partial t$ is estimated from monthly changes in the depth of the 20°C isotherm, and curl $(\tau/\rho f)$ is found from the corresponding wind product. Top panel: western Pacific; middle panel: central Pacific; bottom panel: eastern Pacific.

gradient drove the NECC during 1983. In the NMC wind field (Figure A4) a sharp gradient existed between strong NE Trades and near-zero stress spanning the equator in late 1982-early 1983. The strong (Ekman upwelling) curl associated with this meridional gradient of zonal wind stress kept the model thermocline rising to extremely high levels, hence low dynamic height at 10°N and a strong NECC. The correlation between the terms of the Ekman pumping balance poleward of 10°N was above .8 on the CP and WP tracks for the NMC run (Figure 10).

In the southern hemisphere NMC CP dynamic height varied similarly to that in the north, falling at the end of 1982 similarly to observations but not recovering as the observed dynamic height did in the last half of 1983 (Figure 6). The drop in southern hemisphere dynamic height in late 1982 was in phase with the local Ekman pumping, as was the lack of a recovery in 1983. In mid-1983, while the Sadler winds showed resumption of equatorial easterlies, the NMC winds had near-zero stress spanning the equator; as in the northern hemisphere this pattern led to upwelling curl from the equator to 15°S (Figure A4). Correlation of the Ekman pumping balance was above .8 from 11° to 18°S for the NMC CP, and the CP thermocline continued rising slowly all through 1983 south of the equator in the NMC hindcast. The resulting fall of dynamic height near 10°S led to the development of eastward geostrophic flow (the SECC) early in 1983, as in the XBT observations, but unlike the observations, the model eastward flow persisted and strengthened through 1983 (Figure 7). The meridional profile of zonal geostrophic flow was quite symmetric about the equator in mid-1983, with net transport between 10°S and 10°N strongly eastward, while the XBT observations show net westward geostrophic flow in the same region (Figure 7).

4.3 SADLER

In most regions the SADLER run gave the closest simulation of the XBT observations. On all three tracks, correlations of model vs. observed dynamic heights were as high or higher for the SADLER run than for any of the other hindcasts. SADLER vs. XBT dynamic height correlation were above 0.9 from 15°S to 16°N on the WP track, from 18°S to 4°N on the CP track, and from 5°S to 6°N on the EP track (see Section 5). The amplitude of dynamic height variations in the SADLER run were also generally closer to those observed than were those of the other wind sets (Figures 2 and 6). Near 10°S on the CP track, where the thermocline uplift which caused the largest dynamic height fluctuation observed in the entire XBT data set occurred in early 1983, the SADLER wind set was the only one to reproduce the correct amplitude (Figure 6). In this region, particularly south of 7°S on the CP track (and to a lesser degree in the WP), SADLER model variance was dominated by Ekman pumping, with very high correlations (greater than .95 between 10° and 15°S in the CP) of the Ekman pumping balance (Figure 10). In the northern hemisphere the SADLER variance was similarly controlled by the wind stress curl in the WP and at 10° to 15°N in the CP (Figure 10).

The NECC was too weak through much of the SADLER hindcast, in some areas by as much as a factor of 2. During mid-1983, when the observed NECC was very weak but still present, the model NECC was absent, replaced by weak westward flow (Figure 7).

The SADLER hindcast consistently had the lowest SST of any of the model runs, never developing the extremely high equatorial temperatures typical of most of the other hindcasts (Figure 3). Equatorial SST was underestimated by about 2°C during 1983 on the WP track, by about 5°C during late 1983 on the CP track, and by 2° to 5°C during the entire period on the EP track (Figure 3). Presumably these low surface temperatures were due to the higher mean wind stress in the SADLER product (see Section 3) and consequent higher evaporative heat loss to the atmosphere.

The second downwelling event in the eastern Pacific was best reproduced by the SADLER hindcast, which was the only one of the model runs to show a large second event which was stronger in the lower thermocline than at 22° to 26°C (Figure 5). Thus, this hindcast had the most realistic equatorial dynamic height time series in the EP, with a clear second peak lower than the first (Figure 2), as in the observations.

4.4 FSU

The FSU hindcast was relatively similar to the SADLER run, although the FSU wind stress product used was significantly noisier (see Section 3), and the model results were also noisier, which reduced the monthly correlation with the XBT observations (see Section 5). However, most events which occurred in the SADLER hindcast also occurred in the FSU run. Like the SADLER run, the FSU wind set hindcast a NECC peak in late 1982 which was somewhat weaker than observed and showed a complete cessation of the NECC in mid-1983 (Figure 7). The FSU and SADLER runs were the only two which showed an event of eastward flow near 5°S in the CP in early 1983 which later disappeared as in the XBT observations (Figure 7); the others tended to show this flow continuing through 1983.

The FSU hindcast was generally less dominated by Ekman pumping than was SADLER, with a weaker and less consistent correlation between the terms of the Ekman pumping balance (Figure 10).

Like the SADLER hindcast, the FSU run also tended to have low SST (Figure 3); this is consistent with the higher wind speeds in these two wind products. In the EP, the FSU hindcast a weak first peak of dynamic height and a stronger second peak, unlike the observations (Figure 2). These peaks were associated with two very similar thermocline downwelling events, both involving the entire thermocline unlike the observations; the second peak of dynamic height was higher then the first because of high temperatures in a relatively deep upper layer during March to May 1983 (Figure 5).

4.5 ECMRWF

The ECMRWF experiment produced the best hindcast of variations in the NECC, although in this case as well the peak in late 1982 was too weak. Westward geostrophic flow spanning the equator was hindcast on the CP and WP tracks in 1983 as in the observations, but speeds in the hindcast were higher (Figure 7). The ECMRWF run also produced strong eastward flow near 5°S in the CP persisting through 1983, unlike the observations (Figure 7). This flow was associated with dynamic height near 10°S remaining low, instead of recovering as in the XBT data (Figure 6).

In the EP, the model hindcast a much larger and earlier equatorial dynamic height peak than was observed in the XBT data or any of the other model runs (Figure 2); this was due to the thermocline deepening and upper layer warming which occurred much earlier than in the observations or the other hindcasts (Figures 5 and 3). Possibly the early appearance of warm water in the EP was related to the earlier weakening of the ECMRWF trades on the equator in the CP (Figure A4).

Correlations between the terms of the Ekman pumping balance were more scattered than in the SADLER hindcast, however high correlations were found poleward of about 10°N in the CP and WP and within about 7° of the equator in the WP (Figure 10).

4.6 FNOC

The FNOC wind stresses were consistently the weakest of the five wind products studied (see Section 3), so it is not surprising that dynamic height variance in the model was the smallest in most regions (see Section 5). The time series of dynamic height (Figures 2 and 6) show that the FNOC hindcast produced relatively sluggish fluctuations, particularly in the CP and WP. In addition, zonal geostrophic currents were weaker than in any of the other model runs (Figure 7). The FNOC hindcast had the highest average SST in most locations of any of the runs; this is attributed to low evaporative heat loss in the light FNOC winds. On the equator in the eastern Pacific there was practically no change in the vertical temperature gradient structure (Figure 5). Unlike the other hindcasts or the observations, the FNOC thermocline slowly rose and fell with the vertical temperature gradient relatively constant.

Ekman pumping appeared to have little effect on the FNOC model ocean, except possibly at the far northern end of the CP track (Figure 10).

5. STATISTICAL COMPARISONS

Here we present comparison statistics between the hindcasts and the XBT observations, over the 1982-83 period. Standard deviations and correlation coefficients, of temperature at the surface, 50 meters, 100 meters and 200 meters and of surface dynamic height relative to 450 meters, are the basic comparison parameters. Levels of significance for the correlation coefficients are not easily assigned; there are few degrees of freedom in the two year data set. If we assume that roughly four degrees of freedom are present, which seems reasonable for many of the timeseries, then 95% significance requires correlation greater than 0.81. Correlation coefficients smaller than roughly 0.7 should be regarded as indistinguishable from zero by any reasonable significance standard. As the following discussion will show, there is always quantitative hindcast skill when the correlation exceeds 0.9, and the signal to noise ratio is always found to be less than unity when the correlation is 0.7 or lower.

The hindcast analysis time series were constructed by sampling the full hindcast record once each month, so that high frequency variability (to the extent that it is present) contaminates the hindcast results in a fashion roughly analogous to that in the XBT timeseries, since typically there are only one or two XBTs in each monthly average. The extent to which the XBT timeseries correctly represent the low frequency ocean variability is not addressed here; see Kessler and Taft (1987) for a discussion of error estimates along the central Pacific track. We are not aware of similar error estimates for the eastern and western Pacific tracks. Kessler and Taft (1987) suggest that 0/450 m dynamic height variability is correct to roughly 2 dyn cm; temperature variability is probably correct to within 0.5°C (high frequency noise plus instrumental error) and the (unknown) aliasing error will be a strong function of location and depth. Fortunately the tracks lie outside the region of vigorous 20-30 day variability, so that aliasing of this energy due to the limited sampling is much less a factor than it would be for any meridional section between roughly 110°W and 150°W.

5.1 0/450 m dynamic height

Figure 11 shows the standard deviation of dynamic height from the XBT data for each ship track, to summarize where the variability is greatest and the relative levels of variability during 1982-83. Within the equatorial waveguide the variability increases eastward, from about 7 dyn cm in the WP, to about 11 dyn cm in the CP, to 13 dyn cm maximum in the EP. Along the EP track the greatest variability is within the waveguide, and variability decreases steadily away, to roughly 5 dyn cm at 5°S and 10 dyn cm at 5°N. The CP track has maximum variability of about 14 dyn cm near 8°S with variability decreasing sharply away from the maximum, to the sampling error level at 15°S and to an equatorial plateau of about 11 dyn cm; further north there is a very sharp drop to about 5 dyn cm at 5°N and then a rise to a local maximum of about 8 dyn cm at 10°N. The WP track has maxima at 6°S (13 dyn cm) and 8°N (11 dyn cm), with a

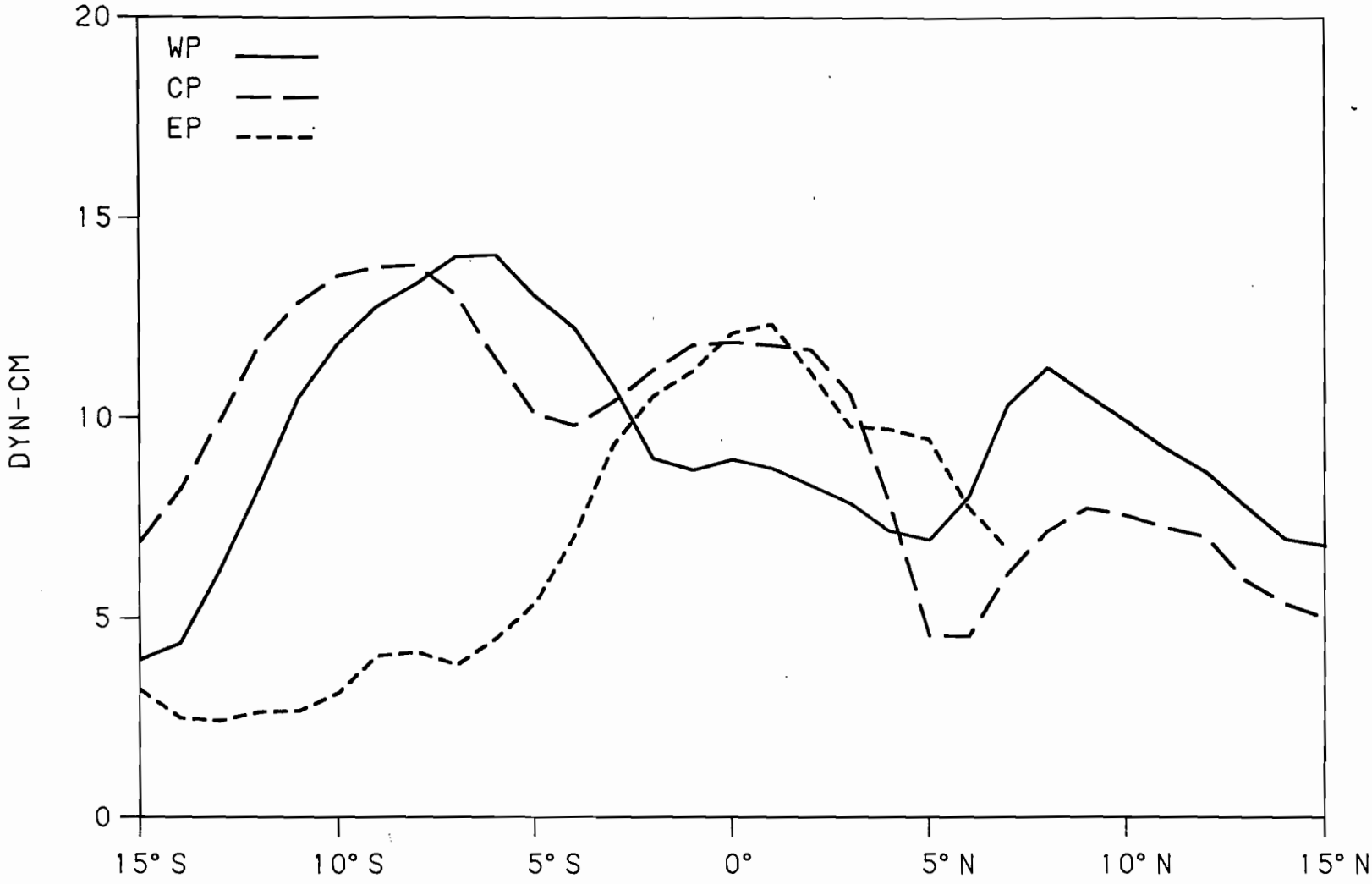

Figure 11: Standard deviation of 0/450 m dynamic height on the three ship tracks from the XBT data.

waveguide plateau (7 dyn cm), a decrease to sampling error at 15°S and a decrease to 5 dyn cm at 15°N. Thus, in addition to the expected waveguide variability, there is strong variability in the NECC (7°-12°N) and between 5° and 10°S in the CP and WP. The particular periods of rapid change have been discussed in Sections 2 and 4.

The model results roughly bracket the EP variability (Figure 14a), with FSU best following the observations and with the SADLER, NMC and ECMRWF cases tending to be more energetic than the observations. Comparing the RMS differences between the different hindcasts and the observations (Figure 14b) shows that SADLER differs the least between 5°S and 5°N and that ECMRWF tends to differ the most, especially north of the equator. Comparing Figure 14a and b indicates that the differences between the hindcasts and the observations are as large as the signal in the data south of 5°S, but that the hindcasts have smaller differences from the data than the signal in the data north of about 2°S. (We shall find it convenient to define the latter situation as "having quantitative hindcast skill" and the former as having "little hindcast skill. When the ratio is less than unity we shall speak of "no hindcast skill", because the noise exceeds the signal.) In other words, the hindcasts have skill in the EP where the signal is strongest, and lack skill once the signal drops to 5 dyn cm or less. Another measure of hindcast performance is the correlation between the hindcast and the observations (Figure 14c). The correlations confirm the skill impressions — north of the equator they are generally greater than 0.8 for each hindcast, and south of the equator the correlations are not significant. The best correlation (exceeding 0.9), where there is skill, is SADLER.

In the CP none of the hindcasts reproduces the observed pattern of variability with great success (Figure 13a). The hindcasts all have a local maximum on the equator, rather than a waveguide plateau, miss the variance minimum at 5°N and the maximum near 10°N (the NMC NECC variance peak will be discussed below). Most have more variance on the equator than at 8°S. Figure 13b shows that there is hindcast skill between 10°S and 3°N for each hindcast, but skill north of 3°N is marginal at best. No hindcast has consistently smallest differences from the data, although SADLER and FSU do relatively consistently well and NMC and ECMRWF do very well within 2 degrees of the equator. There are large hindcast errors in the NECC in NMC. Correlations (Figure 13c) typically exceed 0.8 between 10°S and 2°N, but drop (either somewhat (ECMRWF, SADLER) or precipitously (the others)) by 7°N. Only ECMRWF rises back to marginal significance at 10°N. Each does poorly north of 12°N.

In the WP the NMC, SADLER and ECMRWF runs have variability distributions similar to the observations (Figure 12a). With two exceptions each hindcast has skill between 10°S and 15°N; NMC and FNOC both lack skill in the NECC region. As in the CP, no hindcast consistently has the smallest difference from the data; FNOC does best very near the equator, SADLER is best between 8° and 15°N, etc. Correlation results are less consistent than in the CP, but some very high correlations exist between 2°N and 10°S in NMC, FNOC and SADLER.

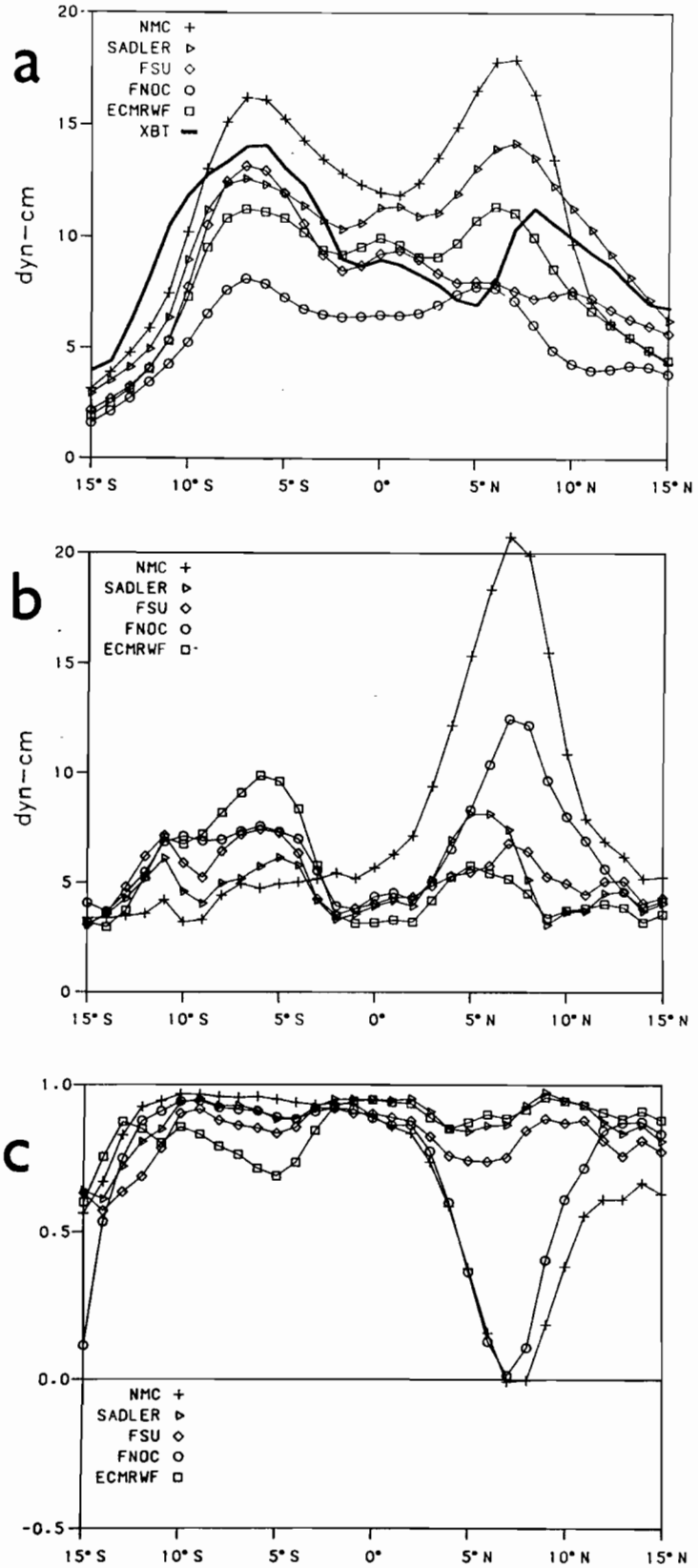

Figure 12: Comparison statistics for 0/450 m dynamic height on the western Pacific track from the XBT data and model hindcasts. a) standard deviation; b) RMS difference between each hindcast and the XBT dynamic height; c) correlation between each hindcast and the XBT dynamic height.

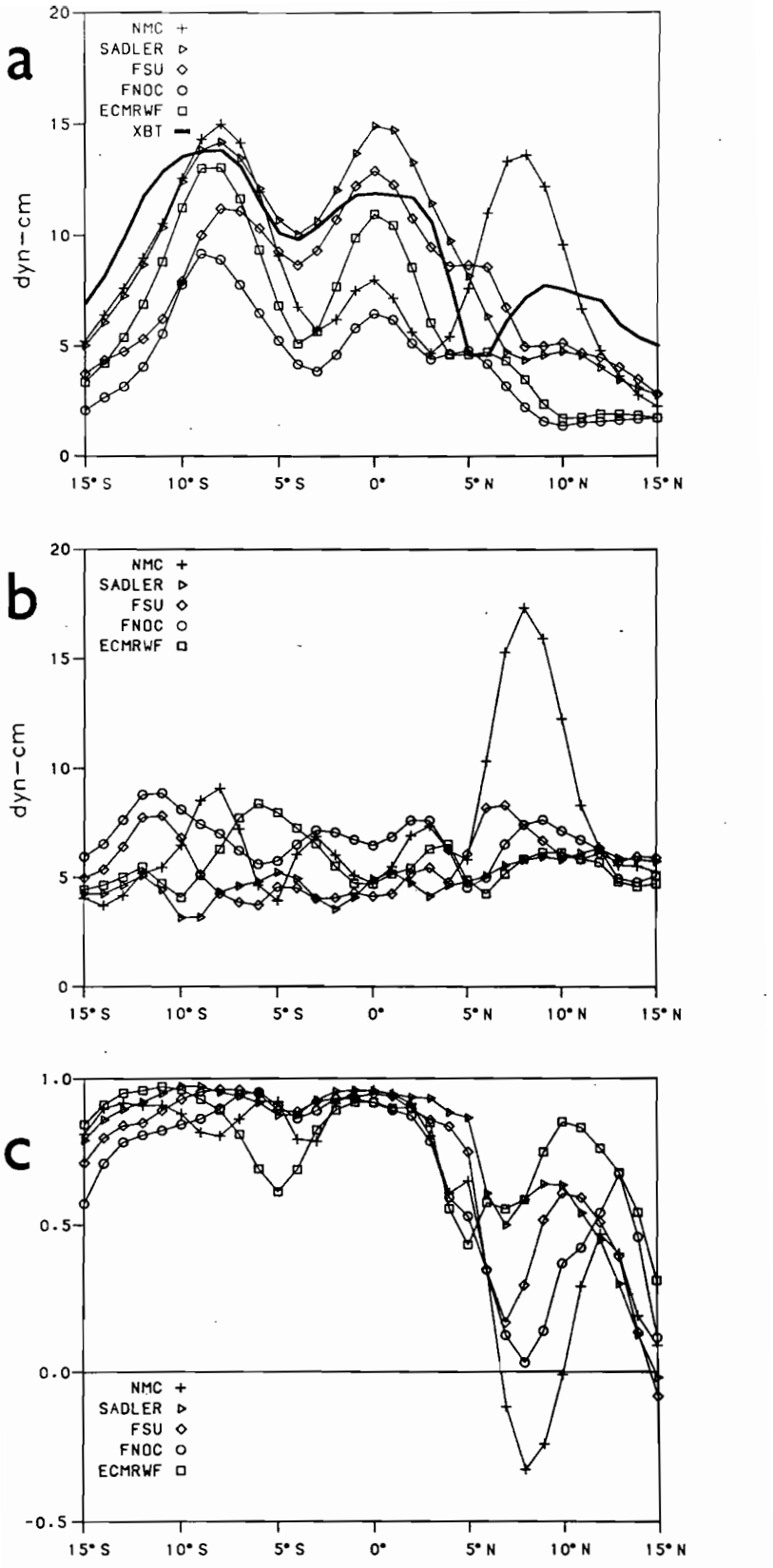

Figure 13: As Figure 12 except for the central Pacific track.

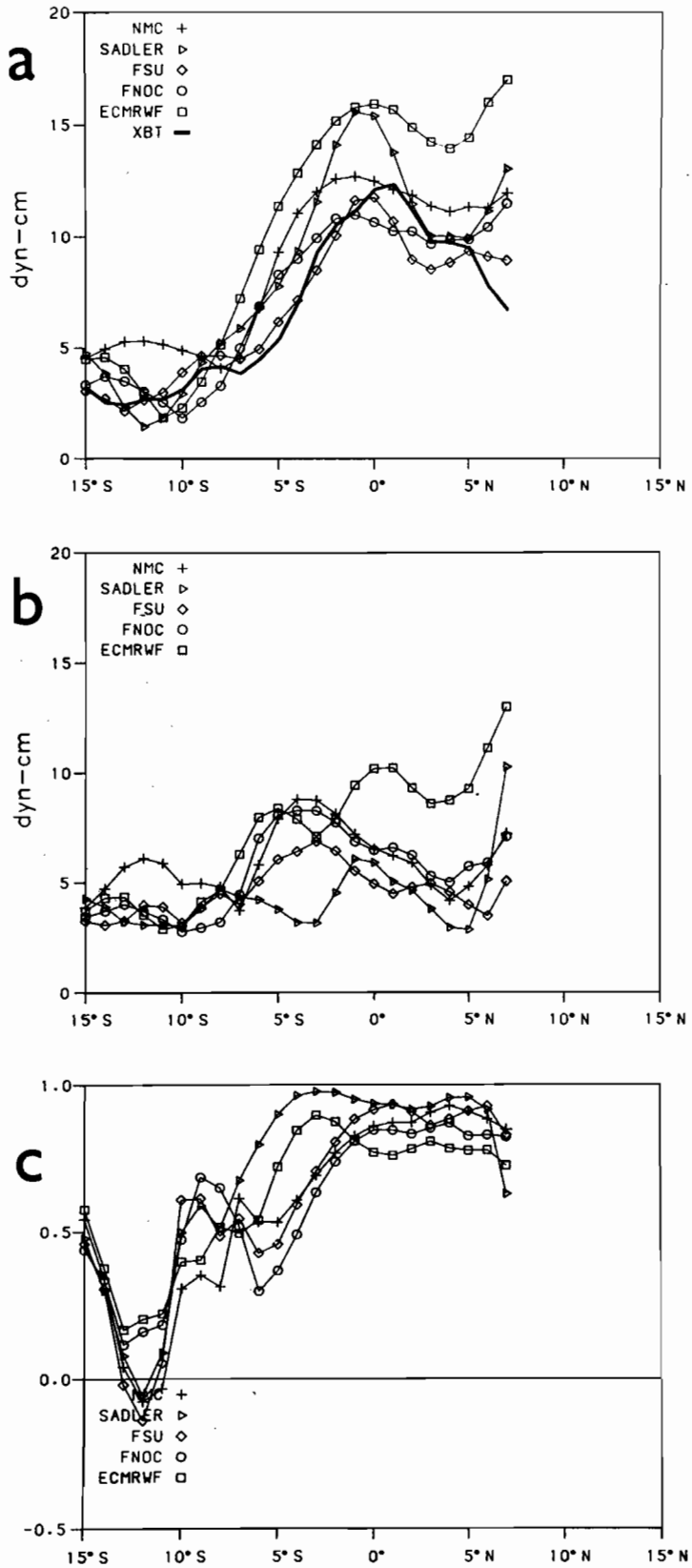

Figure 14: As Figure 12 except for the eastern Pacific track.

To summarize briefly, within 2 degrees of the equator the best hindcasts differ from the XBT data by 2-3 dyn cm RMS (CP and WP) and 4-5 dyn cm (EP), where the RMS signal in the data is 7 dyn cm (WP), 11 dyn cm (CP) and 1114 dyn cm (EP), and correlate with the data at 0.9. The SADLER results are slightly, but consistently, better in the EP; there is little to choose between the better hindcasts in the CP and WP in this latitude range. No simple summary is possible further away from the equator, except that the best hindcasts (which are different for different tracks and different latitudes along a track) differ by 3-5 dyn cm RMS from the data. This represents hindcast skill in places where the variability is large, but not where it is small. Even though there is considerable signal in the NECC region, these latitudes typically correspond to local minima of correlation. Between 5° and 10°S no hindcast does well in the EP, but SADLER does well in the CP, and NMC and SADLER do well in the WP.

A different way of examining the hindcast skill involves comparing the principal modes of variability as revealed by empirical orthogonal function analysis. The EOF modes of dynamic height shown here are renormalized (see Barnett and Patzert (1979)) so that the eigenvectors have dimensions of dyn cm and the time amplitude functions are dimensionless. It suffices here to examine only the first EOF, for the data as well as the hindcasts; typically 80% or more of the variance is contained in the first EOF. Enough of the signal is contained in the first EOF that the amplitude of the EOF is approximately the same as the variability pattern of the data in each case.

The EP EOFs are shown in Figure 15 (lower panels); note that typically 85% of the variance is represented by this EOF. Except for FSU, the hindcast EOFs generally decrease in variance more slowly away from the equator and have more variance at the northern end of the track than does the data EOF; otherwise the shapes are similar. The time evolution for each is shown in Figure 15 on the right. Only SADLER shows roughly constant conditions from January through July 1982, as is seen in the data; FSU decreases from January through March, rises April through May and decreases June-July; FNOC rises February through June, and then is level through August; NMC and ECMRWF rise steadily from February on. The sharp rise occurs in the data in September through December 1982, and is best matched by SADLER. The decrease in January 1983 through March 1983 is present in SADLER and ECMRWF, but is not well matched in the others. The subsequent level period and decrease are present to different degrees in the different hindcasts, but are not matched in any as well as was the late 1982 rise in SADLER.

The CP EOFs and their time histories are shown in Figure 15 (middle panels). As expected from the earlier results, the hindcasts do not correspond so well with the data along this track; although the percent of variance explained is comparable in the hindcasts and in the data, the spatial structures show some considerable differences. The poor hindcast performance between about 5° and 8°N is seen to arise from incorrect phase relationships. Generally the hindcasts

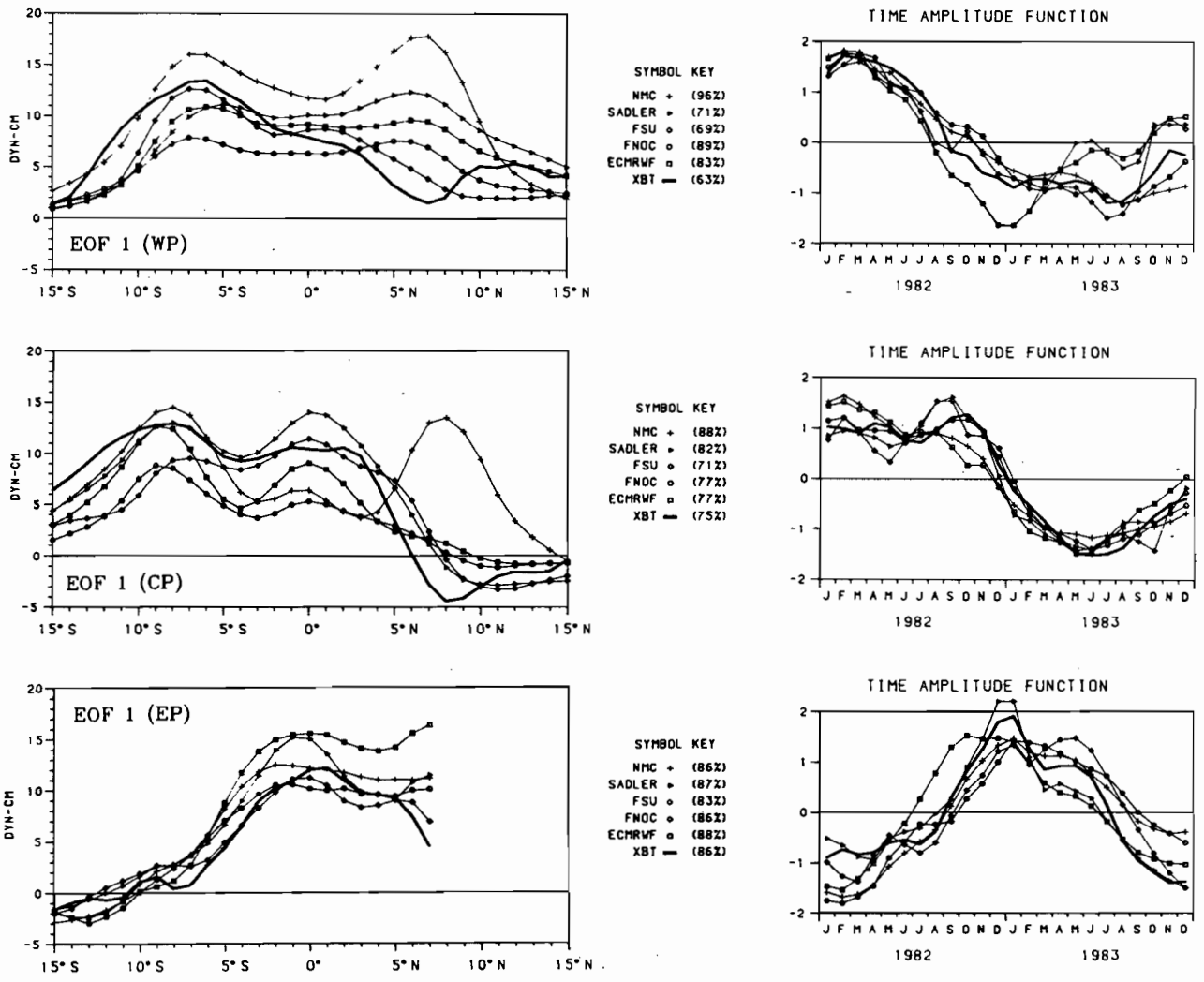

Figure 15: EOF 1 of 0/450 m dynamic height on the three ship tracks from the XBT data and model hindcasts. The EOFs have units of dyn cm and the time amplitude functions are dimensionless. The symbol key in the center shows the percent of total variance represented by EOF 1 in each case. Top panel: western Pacific; middle panel: central Pacific; bottom panel: eastern Pacific.

show more time variability between January 1982 and September 1982 than is seen in the data, but the October through March decline is well simulated by FNOC and FSU. The mid-1983 level period and subsequent rise are generally present in the hindcasts, but are not especially well reproduced by any.

The WP EOFs and their time histories are shown in Figure 15 (upper panels). Note that the data EOF remains positive across the entire latitude range; there is no out of phase region north of 5°N as was found in the CP, although there is still a variance minimum between 5° and 7°N. There are again considerable differences in spatial structure between the hindcast EOFs and the data EOF; note also that the hindcast EOFs account for more of their variance than does the data EOF. There are broad similarities in the time histories; the drop in height is present in each hindcast, but with timing shifts of up to several months, relative to the data.

Similar statistics for the variability of the depth of the 20°C isotherm, which has often been taken as a proxy for thermocline depth variability, were also evaluated. They are so similar in most major aspects to the 0/450 m dynamic height variability that they are not shown.

5.2 Sea surface temperature

The standard deviations of SST, from the XBT data over 1982-83, are shown in Figure 16. As for the dynamic height results, the patterns differ greatly between tracks. Along EP there is a strong equatorial maximum (greater than 2.5°C), with variability dropping off sharply, to less than 1°C poleward of 5 degrees latitude. Along CP there is a waveguide maximum (1.5°C) between minima (about 0.5°C) at 5-6 degrees latitude, and the variability increases poleward of the minima to about 1°C. In the WP the minimum variability (0.7°C) occurs in the waveguide and the variability increases slowly poleward, to more than 1°C.

The hindcast comparisons in the EP are presented in Figure 19. There is a near-equatorial maximum for each hindcast except FNOC, and variability decreases sharply moving northward, but each hindcast seriously overstates the SST variability between the equator and 15°S (see Figure 19a). From the equator northward the hindcast variability is roughly 1°C too large; from the equator southward it can be as much as 2°C too large. Comparing Figure 19a and 19b indicates that there is at best marginal SST hindcast skill, and this only within 2 degrees of the equator and for SADLER, FSU and FNOC. This is further confirmed by Figure 19c, which shows the largest correlation to be barely 0.8 and only very close to the equator (SADLER).

Along the CP track variability is consistently overestimated within 7 degrees of the equator and is generally overestimated elsewhere (Figure 18a). Further, the signal to noise ratio is at best unity and is generally worse (Figures 18a and b), so that there is little quantitative hindcast skill. The smallest RMS differences between the hindcasts and the data near the equator are in NMC (1.5°C); between 3° and 10°N they are in SADLER and NMC (again 1.5°C); well south of the equator there is no best hindcast and differences are typically 1°C. Correlations are best very

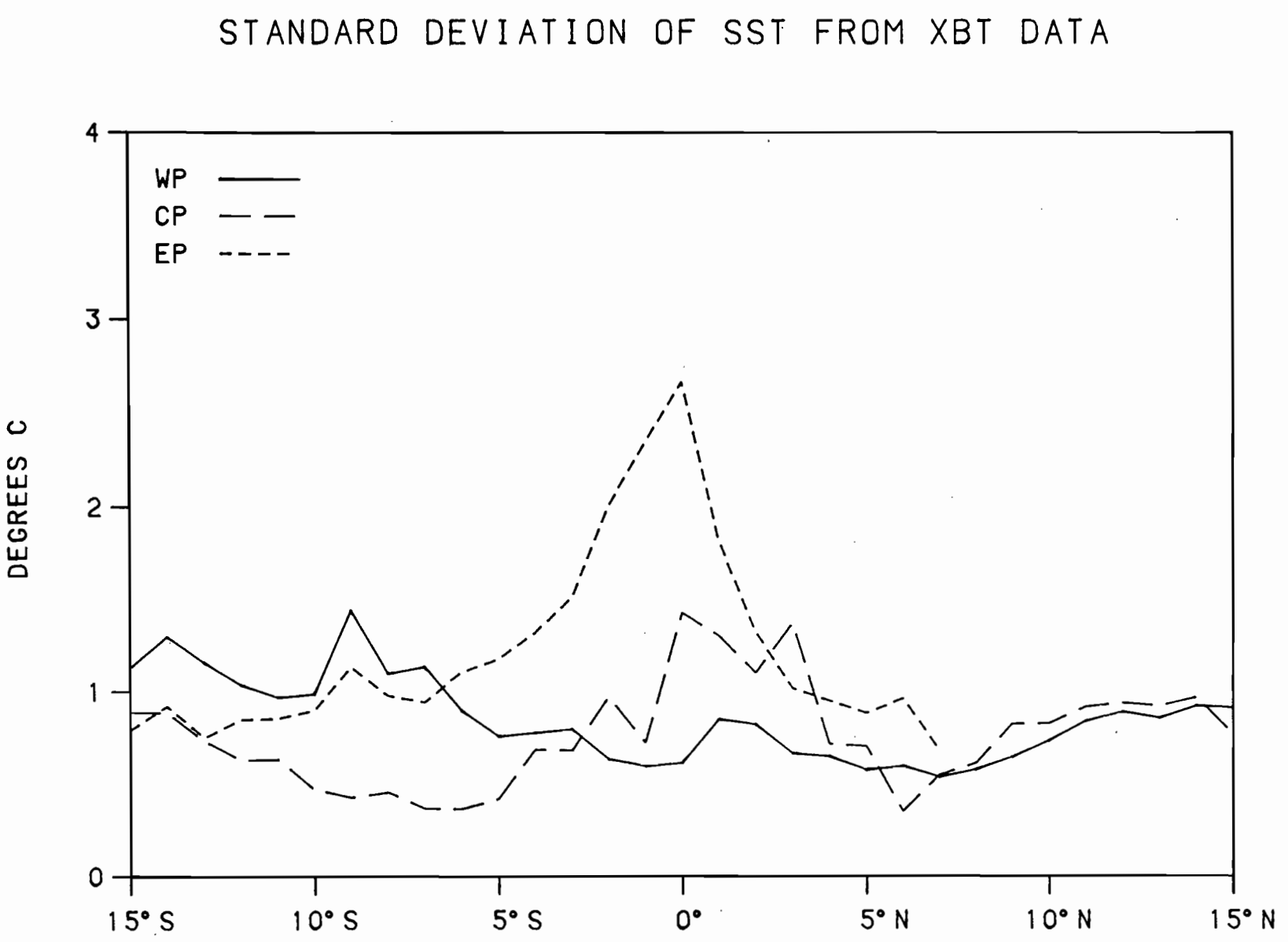

Figure 16: Standard deviation of sea surface temperature on the three ship tracks from the XBT data.

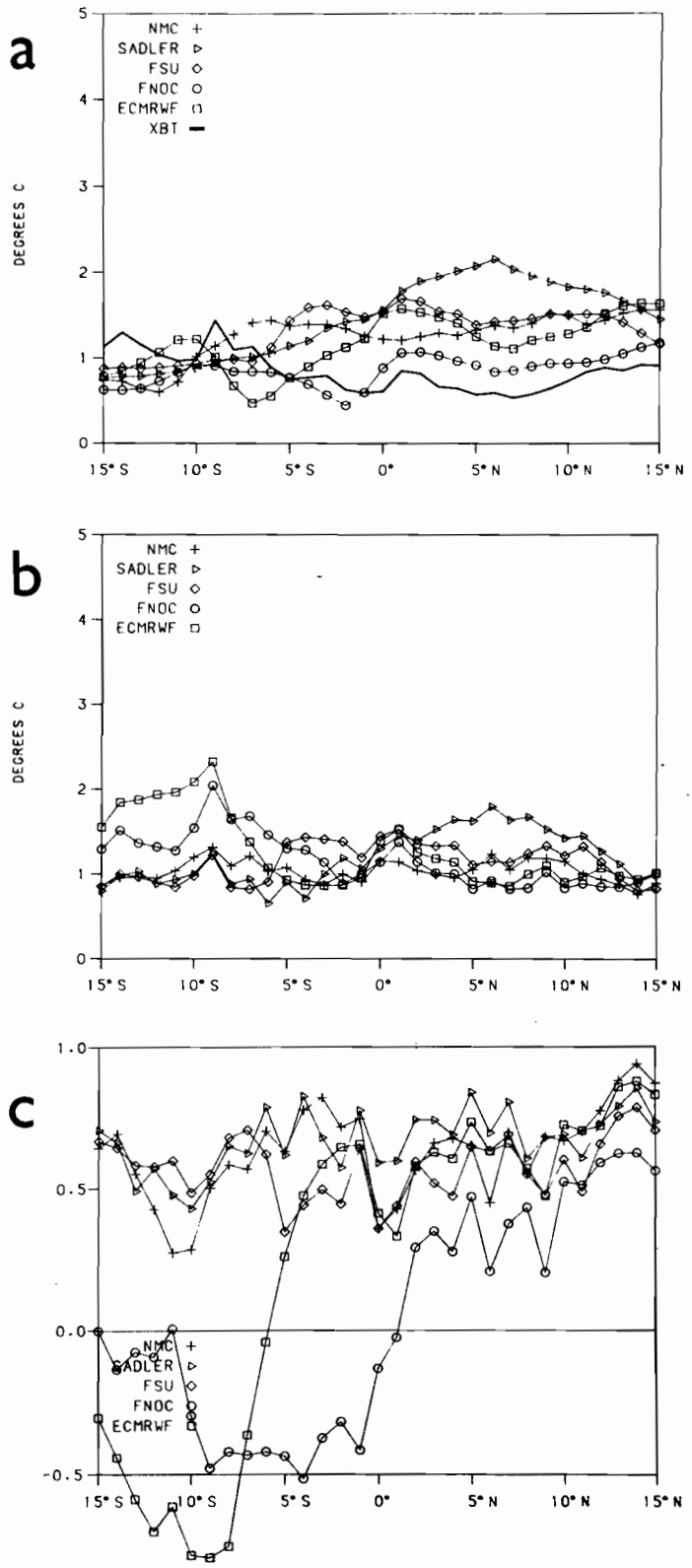

Figure 17: Comparison statistics for sea surface temperature on the western Pacific track from the XBT data and model hindcasts. a) standard deviation; b) RMS difference between each hindcast and the XBT SST; c) correlation between each hindcast and the XBT SST.

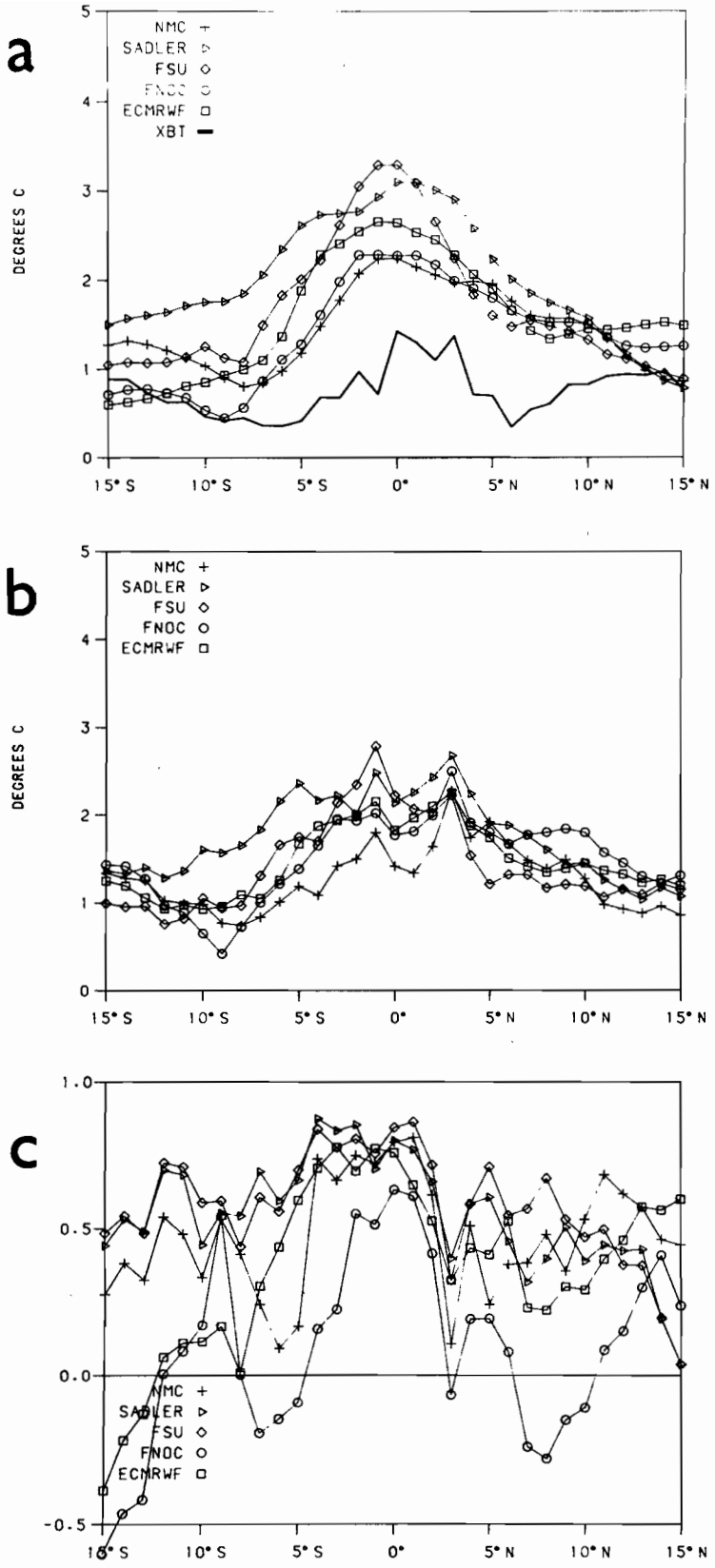

Figure 18: As Figure 17 except for the central Pacific track.

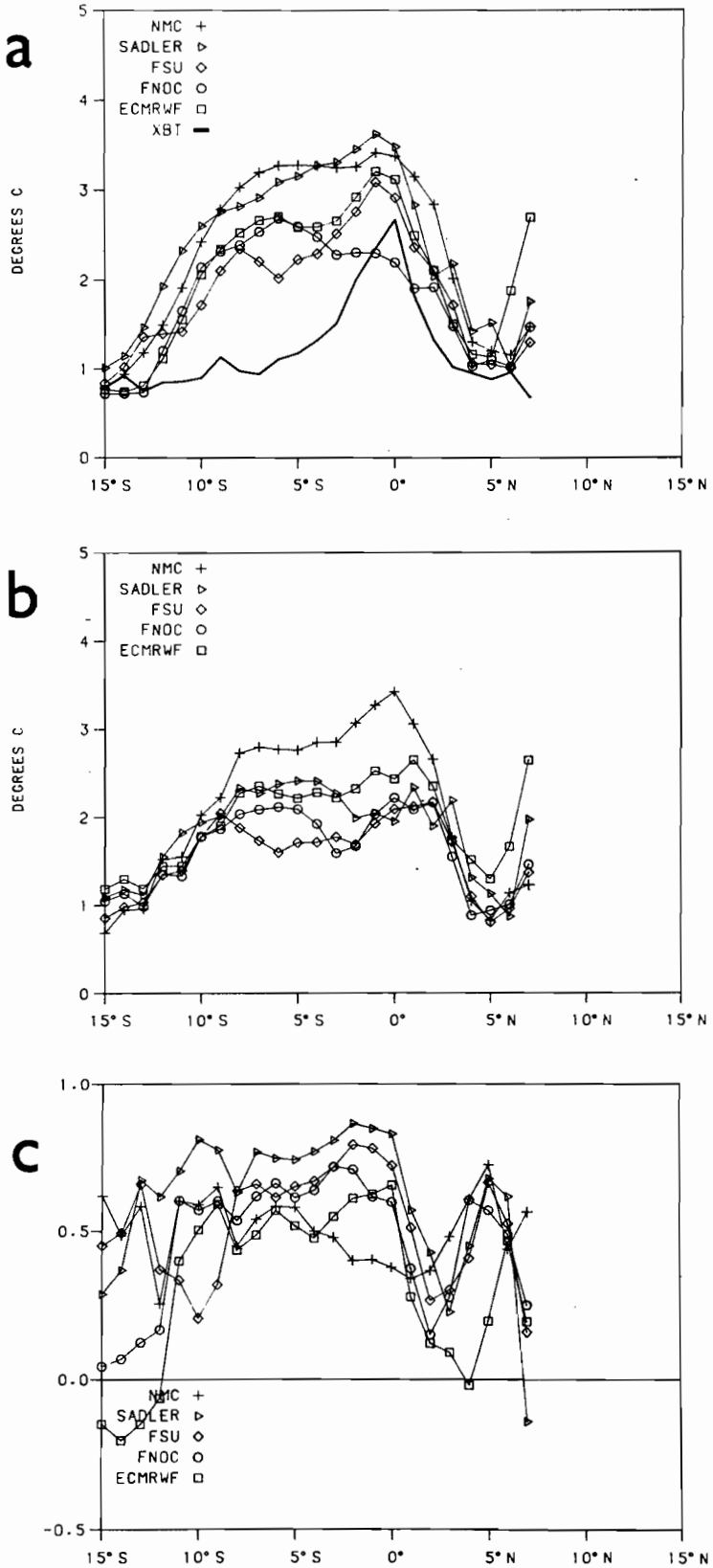

Figure 19: As Figure 17 except for the eastern Pacific track.

near the equator (approaching 0.8 for FSU and NMC), again indicating at best marginal hindcast skill.

In the WP the hindcasts tend to overestimate the variability north of 5°S and to underestimate it south of there (Figure 17a), and the hindcast skill is at best very marginal (signal to noise at best near unity) (Figure 17b). Correlations approach 0.9 between 12° and 15°N for NMC and ECMRWF, but are generally less than 0.7 otherwise (Figure 17c).

Overall then, the SST hindcast skill is far less impressive than the dynamic height skill. RMS hindcast error is at best comparable to the actual signal and is often larger than it. The qualitative character of the hindcasts is correct in almost every case and location – the model ocean warms and cools in rough agreement with the data – but quantitative agreement is seldom found.

5.3 Temperature at 100 m

As is now expected the patterns of T_{100} variability are quite different on the different tracks, but are quite similar to the dynamic height variability in many locations, since both T_{100} and dynamic height variability are due primarily to vertical motion of the thermocline. In the EP there are an equatorial maximum of 4°C, and variability decreases poleward, to roughly 1.5°C at the northern end and to about 0.5°C by 10°S. Along CP there are three maxima, centered at 8°S (2°C), the equator (3.5°C) and 10°N (4°C), separated by minima at 5°S (1.5°C) and 5°N (1°C). Along WP there is a clear maximum at 10°N (4°C), a minimum at 5°N (1.5°C) and a broad shoulder between the Equator and 10°S of 2° to 2.5°C.

The EP hindcast results are shown in Figure 22. Generally variability is underestimated south of the equator and overestimated north of it (Figure 22a). There is at least marginal hindcast skill for most cases between 5°N and 2°S, although ECMRWF has no skill north of the equator (Figure 22b). SADLER has very good skill between 5°S and 2°N, and clearly has the smallest RMS difference from the data between 5°S and the equator. Correlation coefficients show general correspondence between the data and the hindcasts poleward of the equator, but SADLER is the only hindcast to have correlations greater than 0.9.

Along CP the hindcast variability is generally too low, especially poleward of 5 degrees latitude, but also within the waveguide except for SADLER; the southern hemisphere weak maximum is not very well located (Figure 21a). There is generally hindcast skill between 3°N and 10°S, and SADLER has marginal hindcast skill around 8°N (Figure 21b). Correlations show general agreement between 5°N and 12°S; best agreement is within the waveguide and around 10°S (Figure 21c).

In the WP none of the hindcasts captures the strong variability centered near 10°N, but variability levels are less than 0.5°C off between 5°N and 8°S (Figure 20a). There is hindcast skill generally between 3°N and 8°S, and marginal hindcast skill between 8° and 12°N except for

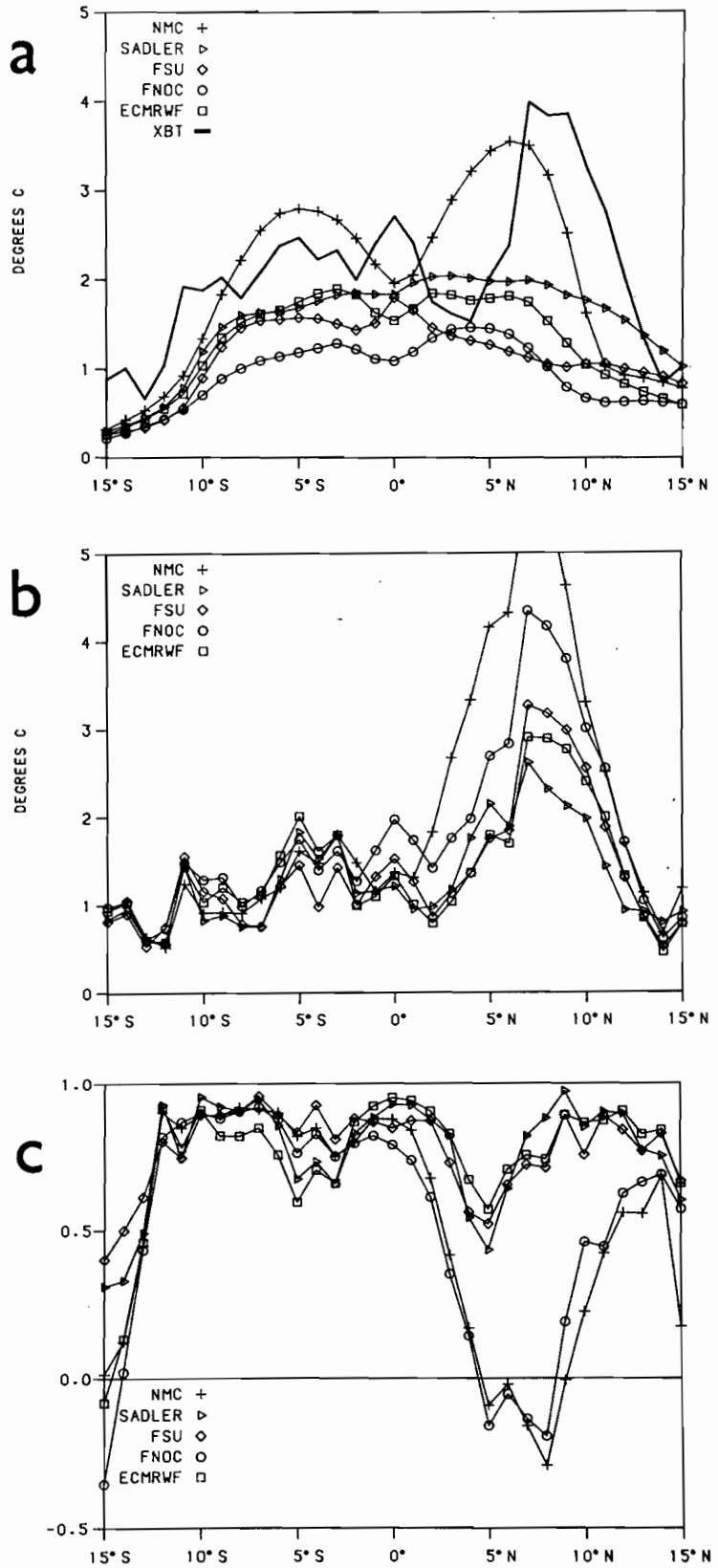

Figure 20: Comparison statistics for temperature at 100 m depth on the western Pacific track from the XBT data and model hindcasts. a) standard deviation; b) RMS difference between each hindcast and the XBT 100 m temperature; c) correlation between each hindcast and the XBT 100 m temperature.

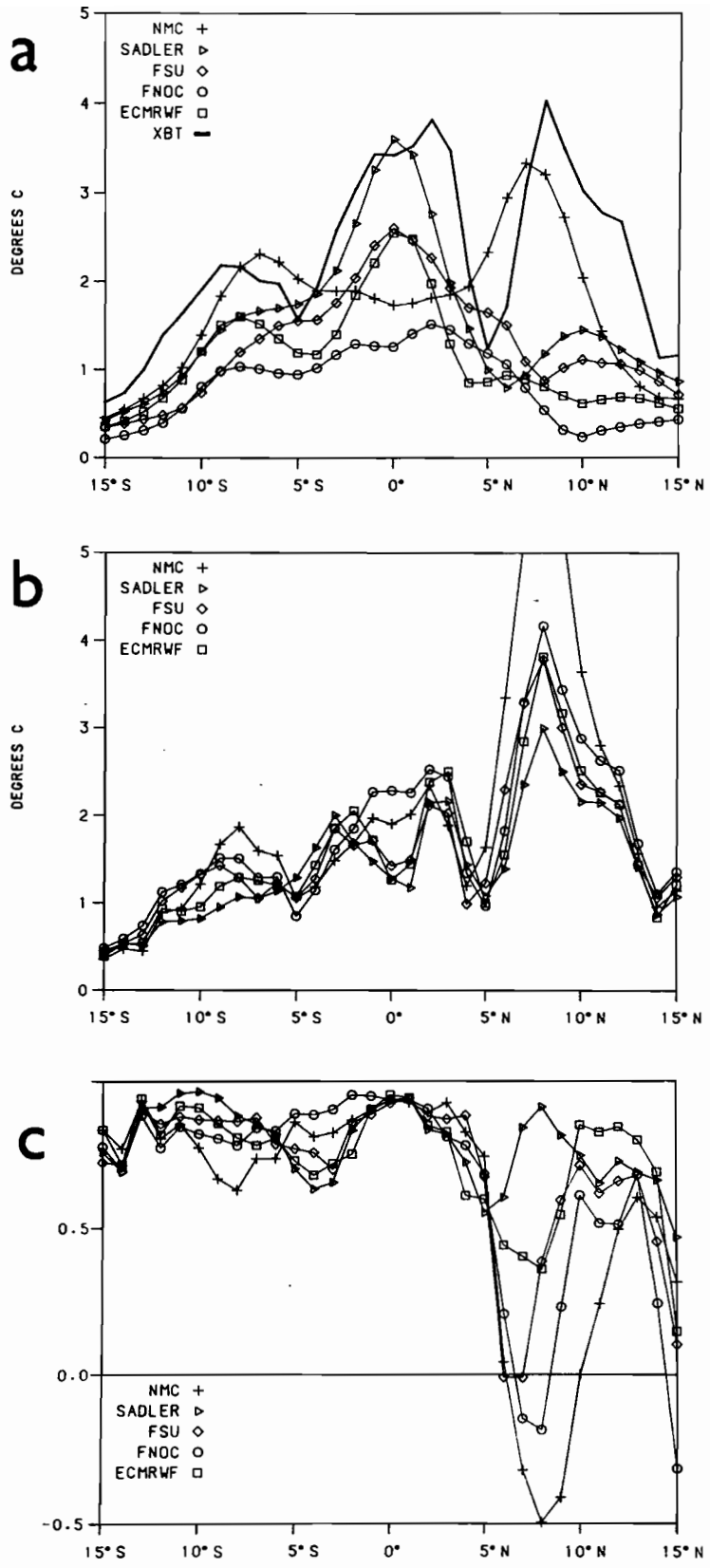

Figure 21: As Figure 20 except for the central Pacific track.

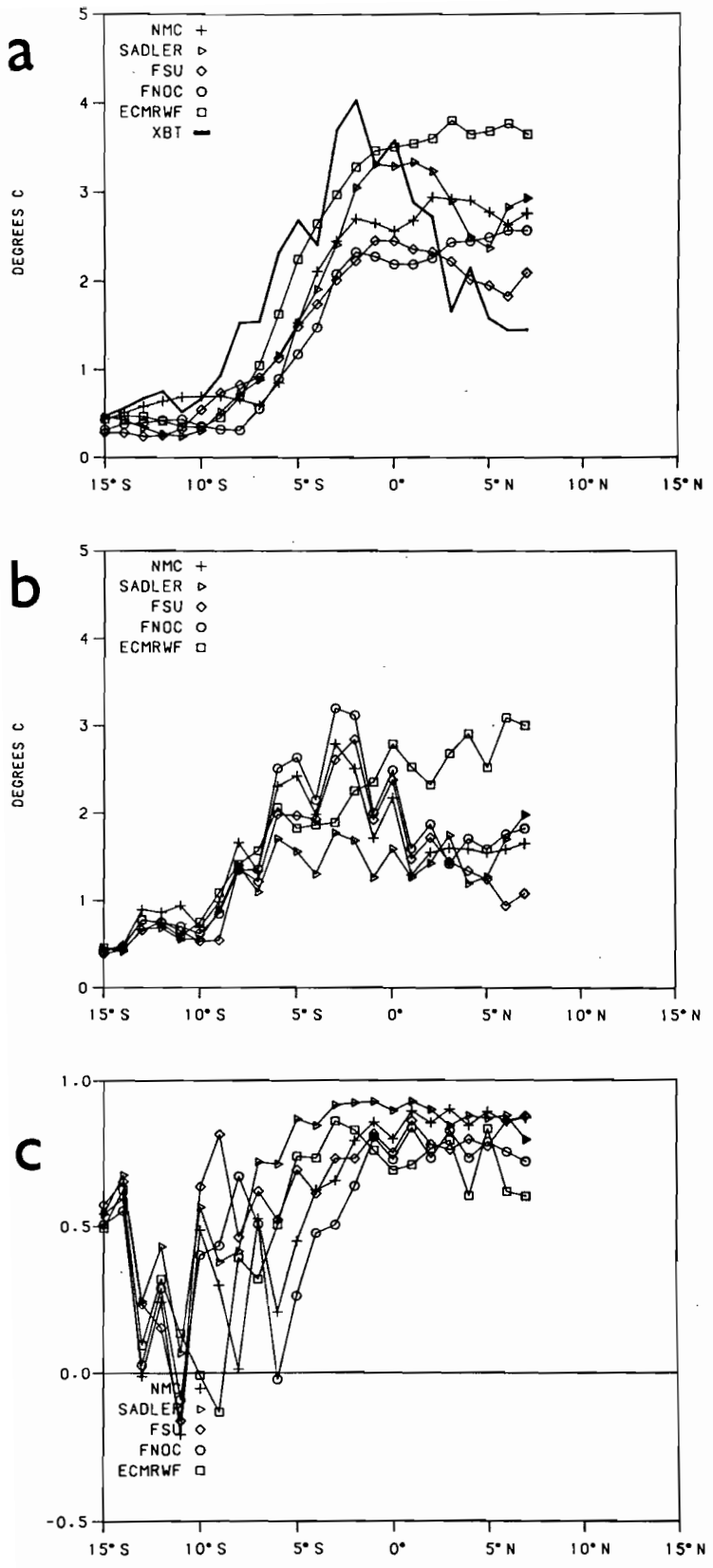

Figure 22: As Figure 21 except for the eastern Pacific track.

NMC and FNOC (Figure 20b). Sadler has the lowest RMS differences with the data between 8° and 12°N; no particular hindcast does best elsewhere. Correlations exceed 0.9 for ECMRWF and SADLER quite close to the equator, often exceed 0.8 between 8° and 12°S for most of the hindcasts, and sometimes exceed 0.8 between 8° and 12°N.

Generally within the waveguide the best hindcasts have RMS differences from the data of about 1°C along WP and 1.5°C along CP and EP. Out of the waveguide the differences are quite spatially variable, but the best signal to noise ratios tend to be between 1 and 2. There is clear hindcast skill for the best hindcasts within the waveguide, and there tends to be hindcast skill in the best cases elsewhere, when the signal in the data exceeds 2°C RMS.

5.4 Temperature at 200 m

The variability patterns of T_{200} along the tracks (not shown) differ greatly from those displayed above; along EP the maximum variability is centered around 10°S and barely exceeds 1°C, along CP the strongest variability occurs in a broad peak centered near 6°S (3.5°C maximum), the near equatorial variability barely exceeds 1°C, there is a minimum around 9°N and the variability then increases slowly northward; in the WP there is again a broad peak centered near 6°S (2.5°C maximum), there is a plateau at about 1°C between the equator and 10°N and then a weaker maximum around 12°N.

The EP hindcast performance is poor. The spatial patterns of variability are not similar to that of the data and basically there is no hindcast skill quantitatively, but only a general weak to modestly positive correlation between hindcast and data.

The patterns of hindcast CP variability include a maximum near 8°S, but otherwise are rather different from that of the data. There is some hindcast skill between 5° and 12°S, and correlation can be as high as 0.9 there (FSU, SADLER). Elsewhere there is no quantitative skill, and correlations are almost always less than 0.7.

Performance is somewhat better in the WP. The hindcast variability patterns pick up the peak and its rough amplitude in the southern hemisphere and the equatorial minimum, but are not consistent with the data north of 5°N. There is some hindcast skill in the southern peak latitudes, and correlations can exceed 0.9 there (FNOC, NMC, SADLER); elsewhere there is qualitative similarity in most hindcasts but no quantitative skill.

6. SUMMARY AND DISCUSSION

Hindcast experiments with the primitive equation tropical pacific ocean general circulation model used by Philander and Seigel (1985) have been performed using five different wind stress analyses for 1982-1983, to investigate hindcast sensitivity to our uncertain knowledge of the wind stress over the tropical Pacific. We use the surface salinity and XBT temperature data collected along three ship tracks, under the French-American ship-of-opportunity program, for

comparison with model hindcast time series along these tracks. Although the monthly average wind stress fields have a number of qualitative similarities, the quantitative differences between analyses are considerable; the different hindcasts reflect these differences in a number of ways, and to differing degrees depending upon the hindcast variable of interest.

The hindcasts of 0/450 m dynamic height variations within the equatorial waveguide were most successful. Each wind stress analysis produced hindcasts with much qualitative similarity to the observations, and most had considerable quantitative skill. In the WP and CP, the best hindcasts correlated with observations at about 0.9; in the EP they are above 0.8. In the WP and CP waveguide the smallest hindcast/data RMS differences approach the estimated observational uncertainty of about 23 dyn cm; in the EP the smallest differences rise to 45 dyn cm. No hindcast consistently produces the smallest RMS differences (see Section 5).

The distinctive double peak in eastern Pacific equatorial dynamic height (Figure 2) has been noted by several investigators who were able to produce double peaks of upper layer thickness with linear, single-active-layer reduced gravity models. Tang and Weisberg (1984), using an idealized wind anomaly, showed that two peaks about 45 days apart at 100°W can be due to the passage of a downwelling Kelvin wave and it's (first meridional mode) Rossby reflection. Such peaks would be too close together to account for the peaks observed in the XBT dynamic height which were five months apart. Tang and Weisberg (1984) also showed that varying the amplitude of the idealized anomaly could produce two separate peaks. This mechanism was borne out by Inoue and O'Brien (1986), who forced their reduced gravity model with the observed FSU winds and found two peaks about 3 months apart which were due to Kelvin waves excited by relatively small-scale variations superimposed on the major westerly wind anomaly. On the other hand, Lukas *et al.* (1984) noted that observed island sea level rose much more slowly in the eastern than in the central Pacific (similar to the XBT dynamic height in our Figure 2), and suggested that these differing shapes of sea level response might be due to modal dispersion from a single large forcing event in the central Pacific, since a second baroclinic mode Kelvin pulse propagates at about half the speed of the first. Our XBT timeseries (Figure 5) show that a single baroclinic mode would give a poor description of the observed variability, particularly during 1983 when highly baroclinic changes occurred, including those associated with the double peak. Most of the model hindcasts, with the exception of FNOC, also showed large changes in the vertical gradient structure in 1983. The double peak signal in the EP is reproduced to some degree in each hindcast, but the second peak is generally not produced for the correct reason; the XBT observations show that the second peak arose both from high upper layer temperature and also large changes in the vertical temperature structure in the lower thermocline and thermostad, while most of the hindcasts (especially NMC) produced it from excessively warm near-surface temperatures. Only the SADLER hindcast clearly had vertical structure changes similar to those in the data.

Dynamic height hindcast skill outside the equatorial waveguide is quite spatially variable (see Sections 4 and 5). Each hindcast has the smallest RMS difference from the data in some region; the SADLER hindcast is never the poorest, which makes it in some sense the most successful. In the WP both north and south of the equator, the best hindcasts do almost as well as the best waveguide hindcasts; in the CP none of the hindcasts has skill near 5°N and even the best have only marginal skill near 10°N, but south of the equator there is generally good skill all the way to 15°S. The SADLER hindcast was best at reproducing the large southern hemisphere changes in both the CP and the WP. There is no hindcast skill outside the waveguide along the EP track.

A very simple examination of the extent to which direct wind stress curl forcing of thermocline depth changes is taking place (via Ekman pumping) suggests that this can be a major factor in the dynamic height changes outside the waveguide; the large changes in NECC transport and in SEC transport in the CP and WP appear to result largely from the large changes in wind stress curl which themselves arise from the changes in the stress within 10 degrees of the equator. Of course, adjustment outside the waveguide generally involves slower processes than within the waveguide, and adjustment from initial condition shock is still taking place at the end of these hindcasts, but we find that the strong stress analyses create sufficiently strong direct forcing to give clear Ekman pumping response. This indicates that the problems in hindcast skill in the NECC region are importantly affected by the deficiencies in the wind stress curl patterns implicit in the monthly mean stress analyses.

SST hindcast skill was at best qualitative. Generally the ocean warmed and cooled roughly in phase with the changes in the ocean, particularly within the waveguide, but RMS differences between the hindcasts and the observations almost always exceeded the RMS signal in the data. The strong stress hindcasts (SADLER and FSU) tended to produce colder SST than was observed in the eastern and central equatorial Pacific when the SE Trades were present, while the weaker stress analyses (NMC, FNOC and ECMRWF) tended to have SST too high in the western and central Pacific. Thus unrealistic SST, and SST gradients, existed in all of the hindcasts much of the time.

Equatorial SST changes are determined by the competing interaction of many processes – horizontal and vertical advection, mixed layer depth changes, mixing and surface heat flux – so that it is a particularly difficult variable to hindcast. Both the vertical mixing and surface heat flux parameterizations require further investigation and improvement; under light wind conditions the model SST values commonly approached 32°C or even higher. Any physically based parameterization of the surface heat flux (as opposed to a Haney (1974) type empirical parameterization) will depend upon knowledge of the surface wind speed (which enters the bulk formula expressions for both the sensible and latent heat flux components) and any quasi-bulk layer mixed layer model will depend upon the kinetic energy input to the layer, which depends

upon the magnitude of the wind stress. Clearly, surface wind and wind stress uncertainty has a major influence on hindcast SST skill.

Subsurface temperature hindcast skill is good where temperature changes roughly are correlated with thermocline depth changes. Where there are changes in the vertical structure of the temperature between the surface and the thermocline, hindcast skill is highly variable and generally not high.

Sea surface salinity is very poorly hindcast. Both air-sea and zonal advective fluxes of salt and water contributed to large salinity changes observed in the ship of opportunity data. There is no parameterization of precipitation minus evaporation in the model physics, so any changes due to surface liquid water flux are absent from the model. Further, the Philander and Seigel (1985) initial state of the model ocean does not have realistic surface salinity gradients, so advective changes are also missed in the hindcasts. We can only speculate that the model mixing processes affecting salinity have eliminated most of the horizontal salinity gradients in the course of the Philander and Seigel (1985) spin-up to the initial state used in these experiments. As salinity effects are not unimportant in the data, improvement of treatment of salinity in the model also deserves attention.

It is important to note that the different stress fields are not direct output of any of the research or operational wind or pseudostress analyses; rather we, or others, have taken analysis products and converted them to wind stress fields according to our judgements. The choice of $C_d = 1.2 \times 10^{-3}$ for the SADLER and FNOC conversions is not conventional, but is based on the fact that this value gave better hindcast results than did larger values. The choices made to convert FNOC winds to stress resulted in quite small stress values; we have not attempted to determine if the FNOC winds are much smaller than the winds used in other analyses. The NMC conversion was made by Philander and Seigel (1985) and the ECMRWF conversion was made by N. Wells. The hindcasts indicate that SST hindcast skill is very sensitive to the magnitude of the zonal stress near the equator, and that off-equatorial variability is strongly affected by wind stress curl amplitude and pattern, so there are significant issues associated with how wind analyses ought to be converted to stress fields. At this time these issues are far from clear.

Earlier hindcast studies of interannual variability in the tropical Pacific (e.g., Busalacchi and O'Brien (1979), Busalacchi and Cane (1985) have found that waveguide dynamic height variation can be hindcast with some skill even with simple linear model physics and complete neglect of thermodynamics. Most of these studies have made use of the FSU pseudostress analysis. Quantitative hindcast skill has not been discussed, except in terms of simple correlation coefficients. Efforts to improve on the skill of simple single mode linear reduced gravity models have led to uncertainty about how wave speeds should be chosen, and how the variable background density structure should be felt in the models.

This study shows that major waveguide dynamic height changes like those that took place in 1982-83 can be hindcast with any of the available monthly mean surface stress analyses, and that no single analysis produces the best hindcast even throughout the waveguide. The sea surface temperature and vertical temperature structure changes that occurred are large, and the inclusion of primitive equation physics appears necessary to an understanding of these changes. Outside of the waveguide wind stress curl has been found to play an important role in the observed changes and in the model changes, so the relatively poor hindcast skill in the NECC appears directly related to the very uncertain wind stress curl fields in this region. Generally the special research products (FSU and SADLER) have higher skill in this region, which presumably results from their better spatial resolution of the wind stress there. The FSU analysis hindcast generally has poorer correspondence with the data than the SADLER hindcast; we attribute this to the greater month-to-month and region-to-region changes in the FSU analysis, since the gross aspects of the two analyses are very similar. Both the SADLER and FSU hindcasts have larger SST errors than the operational stress analysis hindcasts.

It has been suggested that the genesis of the 1982-83 El Niño involved a westward propagating baroclinic disturbance that was seen well north of the equator in 1981 (White *et al.*, 1985; Pazan *et al.*, 1986; Inoue *et al.*, 1987). We note that all of the hindcasts described here were initialized with simulated climatological January conditions which included no information from the Pacific in 1981. The fact that good to excellent hindcasts of waveguide dynamic height were obtained here (Sections 4 and 5) indicates that the primary El Niño waveguide signal was contained in the 1982-83 wind stress changes and not in the free evolution of 1981 subsurface conditions.

Although elements of the ocean circulation model physical parameterizations, and the model initial conditions require improvement, these results indicate a very clear need for improved knowledge of the surface wind stress field over the tropical Pacific if we are to achieve quantitative hindcast skill for the ocean thermal quantities of interest in the El Niño phenomenon.

7. ACKNOWLEDGMENTS

The interest, support and assistance of G. Philander and R. Pacanowski, who made their model available and helped us set it up on the NBS/NOAA Cyber 205, saved us many months of effort and is gratefully acknowledged. The various wind fields were made available to us by J. O'Brien (FSU), N. Wells (ECMRWF), A. Seigel (NMC), J. Sadler (SADLER) and the Fleet Numerical Ocean Central of the US Navy (FNOC); thanks to all; it must be noted that all decisions concerning how to convert the FNOC, SADLER and FSU fields to stress were made by the authors. The ship of opportunity program was initiated by G. Meyers, W. White, J.-R. Donguy and D. Cutchin and has been continued as a cooperative program by the Office de la Recherche Scientifique et Technique Outre-Mer and the Scripps Institution of Oceanography. Computer

time to carry out the model experiments on the NBS/NOAA system was provided by V. Derr of NOAA/ERL; J. Coffee, J. Harper and the computer center staff and operators made many special efforts to assist our getting this accomplished in as timely a way as possible. The expert programming assistance of S. Hankin and M. Verschell at PMEL, and PMEL computing support were also essential. The U.S. TOGA Project Office provided partial start-up support, and subsequent partial support has been received from the NOAA EPOCS Program. The financial support and enthusiasm of E. Bernard, Director of PMEL, are very much appreciated.

8. REFERENCES

Bunker, A.F., 1976: Computations of surface energy flux and annual air-sea interaction cycles of the North Atlantic Ocean. *Mon. Wea. Rev., 101*, 1122-1140.

Barnett, T.P. and W.C. Patzert, 1980: Scales of thermal variability in the tropical Pacific. *J. Phys. Oceanogr., 10*, 529-539.

Busalacchi, A.J. and J.J. O'Brien, 1981: Interannual variability of the equatorial Pacific in the 1960's. *J. Geophys. Res., 86*, 10901-10907.

Busalacchi, A.J. and M. Cane, 1985: Hindcasts of sea level variations during the 1982-83 El Niño. *J. Phys. Oceanogr., 15*, 213-221.

Firing, E., R. Lukas, J. Sadler and K. Wyrtki, 1983: Equatorial Undercurrent disappears during 1982-83 El Niño. *Science, 222*, 1121-1123.

Goldenberg, S.B. and J.J. O'Brien, 1981: Time and space variability of tropical Pacific wind stress. *Mon. Wea. Rev., 109*, 1190-1207.

Halpern, D., D.E. Harrison, B. Hinton, R. Long, M. Mathur, J. O'Brien, S. Payne, S. Pazan, and J. Sadler, 1982: Intercomparison of November 1979 Pacific tropical surface winds. MIT Dept. of Meteorology and Physical Oceanography, Technical Report 82-1, 40 pp.

Harrison, D.E., 1984: On the appearance of sustained equatorial westerlies during the 1982 Pacific warm event. *Science, 224*, 1099-1102.

Harrison, D.E., V. Cardone, J.J. O'Brien, D. Reynolds, J. Sadler and D. Wylie, 1984: Report of the ad hoc committee on surface wind and wind stress fields. Univ. Corp. for Atmos. Res., USTOGA 2, 49 pp.

Haney, R., 1974: A numerical study of the response of an idealized ocean to large scale surface heat and momentum flux. *J. Phys. Oceanogr., 4*, 145-167.

Hellerman, S. and M. Rosenstein, 1983: Normal monthly wind stress over the world ocean with error estimates. *J. Phys. Oceanogr., 13*, 1093-1104.

Inoue, M. and J.J. O'Brien, 1986: Predictability of the decay of the 1982/83 El Niño. *Mon. Wea. Rev., 114*, 967-972.

Inoue, M., W.B. White and S.E. Pazan, 1987: Interannual variability in the tropical Pacific prior to the onset of the 1982-83 El Niño. *J. Geophys. Res.*, (in press).

Kessler, W.S., B.A. Taft and M. McPhaden, 1985: An assessment of the XBT sampling network in the central Pacific. Univ. Corp. for Atmos. Res., USTOGA 4, 62 pp.

Kessler, W.S. and B.A. Taft, 1987: Dynamic heights and zonal geostrophic transports in the central tropical Pacific during 1979-84. *J. Phys. Oceanogr., 17*, 97-122.

Large, W.G. and S. Pond, 1981: Open ocean momentum flux measurements in moderate to strong winds. *J. Phys. Oceanogr., 11*, 324-336.

Levitus, S., 1982: *Climatological Atlas of the World Ocean.* NOAA Prof. Paper 13, U.S. Govt. Printing Office, Washington, D.C., 173 pp., 17 microfiche.

Lukas, R., S.P. Hayes and K. Wyrtki, 1984: Equatorial sea level during the 1982-1983 El Niño. *J. Geophys. Res., 89*, 10425-10430.

Luther, D.S. and D.E. Harrison, 1983: Observing long-period fluctuations of surface winds in the tropical Pacific: initial results from island data. *Mon. Wea. Rev., 112*, 285-302.

Meyers, G., 1979: On the annual Rossby wave in the tropical North Pacific Ocean. *J. Phys. Oceanogr., 9*, 663-674.

McPhaden, M.J., Busalacchi, A.J., Picaut, J. and G. Raymond, 1987: Aliasing of zonal variability in the tropical Pacific ship-of-opportunity program. Submitted to *J. Geophys. Res.*

Niiler, P.P. (editor), 1981: Tropical Pacific upper ocean heat and mass budgets. A research program outline. Hawaii Institute of Geophysics Special Publication, 56 pp.

Pazan, S.E., W.B. White, M. Inoue and J.J. O'Brien, 1986: Off-equatorial influence upon Pacific equatorial dynamic height variability during the 1982-83 ENSO event. *J. Geophys. Res., 91*, 8437-8449.

Philander, S.G.H. and A.D. Siegel, 1985: Simulation of El Niño of 1982-1983. *Coupled Ocean-Atmosphere Models*, J. Nihoul, Ed., Elsevier, 517-541.

Philander, S.G.H., W.J. Hurlin and R.C. Pacanowski, 1987: Initial conditions for a general circulation model of tropical oceans. *J. Phys. Oceanogr., 17*, 147-157.

Rasmussen, E.M. and T.H. Carpenter, 1982: Variations in tropical sea surface temperature and surface wind fields associated with the Southern Oscillation-El Niño. *Mon. Wea. Rev., 110*, 354-384.

Rebert, J.P., J.-R. Donguy, G. Eldin and K. Wyrtki, 1985: Relations between sea level, thermocline depth, heat content and dynamic height in the tropical Pacific Ocean. *J. Geophys. Res., 90*, 11719-11725.

Sadler, J. and B.J. Kilonsky, 1983: Meteorological events in the central Pacific during 1983 associated with the 1982-83 El Niño. *Trop. Ocean-Atmos. Newslett., 21*, 3-5.

Sadler, J. and B.J. Kilonsky, 1985: Deriving surface winds from satellite observations of low-level cloud motions. *J. Climate Appl. Meteor., 24*, 758-769.

Schopf, P.S. and M.A. Cane, 1983: On equatorial dynamics, mixed layer physics and sea surface temperature. *J. Phys. Oceanogr., 13*, 917-935.

Schopf, P.S. and D.E. Harrison, 1983: On equatorial waves and El Niño. I: Influence of initial states on wave-induced currents and warming. *J. Phys. Oceanogr., 13*, 936-948.

Tang, T.Y. and R.H. Weisberg, 1984: On the equatorial Pacific response to the 1982-1983 El Niño-Southern Oscillation event. *J. Mar. Res., 42*, 809-829.

White, W.B., G. Meyers, J.-R. Donguy, S. Pazan, 1985: Short-term climatic variability in the thermal structure of the Pacific Ocean during 1979-82. *J. Phys. Oceanogr., 15*, 917-935.

Wyrtki, K., 1984: The slope of sea level along the equator during the 1982/1983 El Niño. *J. Geophys. Res., 89*, 10419-10424.

Wyrtki, K., 1984b: A southward displacement of the subtropical gyre in the South Pacific during the 1982-83 El Niño. *Trop. Ocean-Atmos. Newslett., 23*, 14-15.

Wyrtki, K. and G. Meyers, 1975: The trade wind field over the Pacific. Part II: Bimonthly fields of wind stress, 1950-1972. University of Hawaii. Ref. HIG-75-2, 16 pp. plus appendix.

Wyrtki, K. and B.J. Kilonsky, 1984: Mean water and current structure during the Hawaii-to-Tahiti Shuttle Experiment. *J. Phys. Oceanogr., 14*, 242-254.

APPENDIX: 1982-83 Surface wind stress fields and comparison statistics

We here present a variety of figures to summarize the features of the wind stress fields during 1982-83 along the ship tracks (see Figure 1), and the differences between them. Figures are grouped by ship track (A.1-A.3 for the WP, A.4-A.6 for the CP and A.7-A.9 for the EP). The first figure for each track presents the 1982-83 monthly mean vector surface stresses, as well as the corresponding Hellerman and Rosenstein (1983) climatological stresses (which were used to spin the model up to the initial state of the hindcasts). The next figure presents the 1982-83 time averages and standard deviations about the averages for zonal and meridional stress: these statistics provide measures of the offsets between stress fields and of the total stress variation experienced over 1982-83 in each analysis. To add a different perspective on the differences between stress fields, the final figure for each ship track presents comparison statistics, using the SADLER stress analysis as a baseline about which standard deviations and correlation coefficients are evaluated for each of the other stress fields.

The interested reader is encouraged to browse the figures for the quantitative comparisons of most particular interest (see also Section 3 for some specific discussion of the wind fields and departures from climatological conditions). Unfortunately no general discussion is possible; there is generally large variability in the comparison between any two analyses from track to track. That there is considerable qualitative similarity between analyses is clear from the generally positive correlations between SADLER and the other analyses, but there are tracks and latitudes where correlation can be quite small. The SADLER and FSU analyses tend to be the most similar of any two analyses, with FSU tending to be smaller than SADLER by 0.1 to 0.2 dyne cm^{-2} in the mean and to have smaller RMS variability about its mean by about 0.1 dyne cm^{-2}. The differences between other analyses and their variability over 82-83 are generally significantly greater; in the CP NECC region mean zonal and meridional stress differences can each exceed 0.3 dyn cm^{-2}.

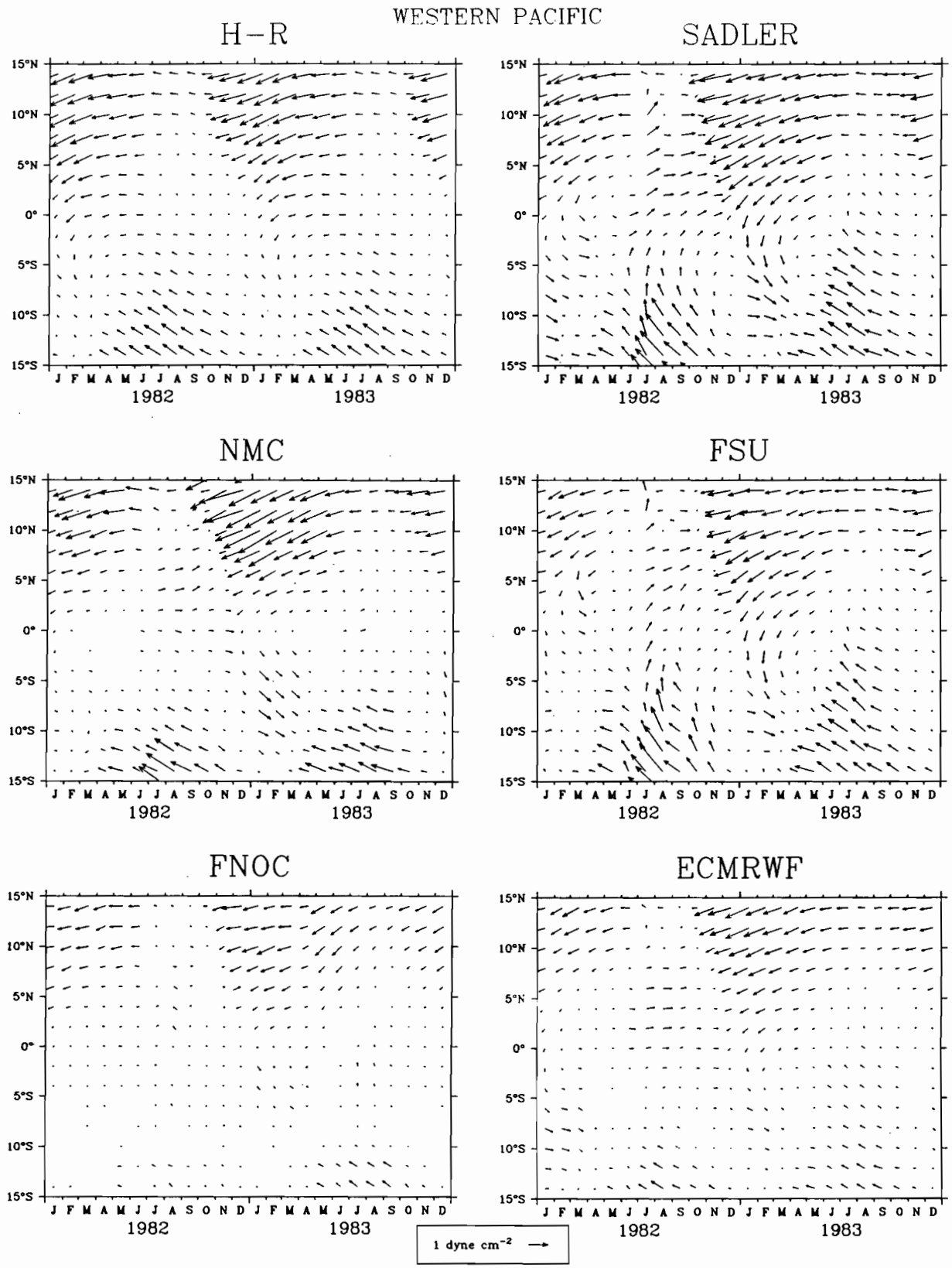

Figure A1: Monthly mean surface wind stress vectors on the western Pacific track from the Hellerman and Rosenstein (1983) climatology and the five wind products studied. The scale vector at bottom center indicates 1 dyn cm^{-2}.

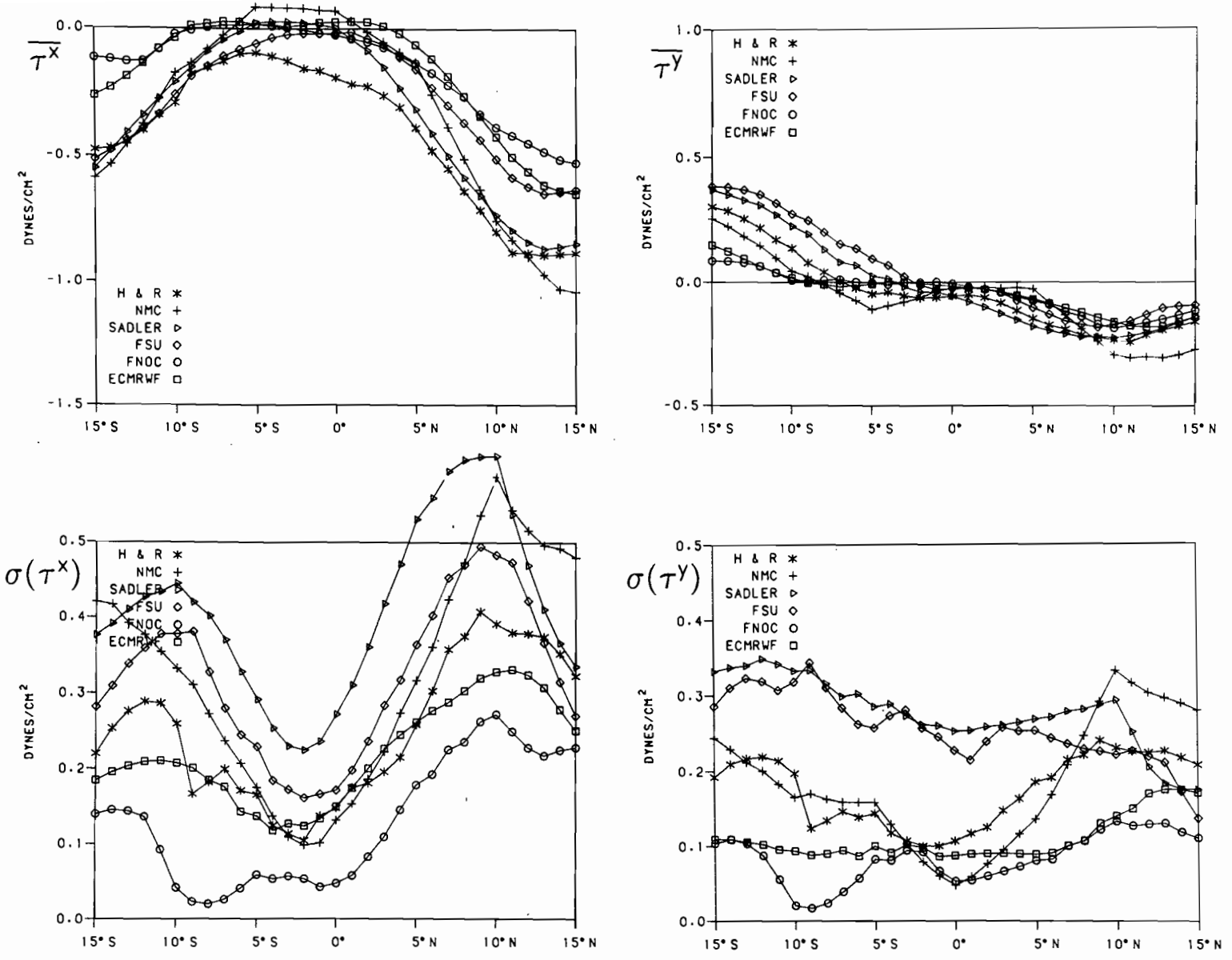

Figure A2: Mean and standard deviation of zonal and meridional wind stress on the western Pacific track from the Hellerman and Rosenstein (1983) climatology and the five wind products studied, for the period 1982-83. Left panels: τ^x; right panels: τ^y. Top panels: mean; bottom panels: standard deviation.

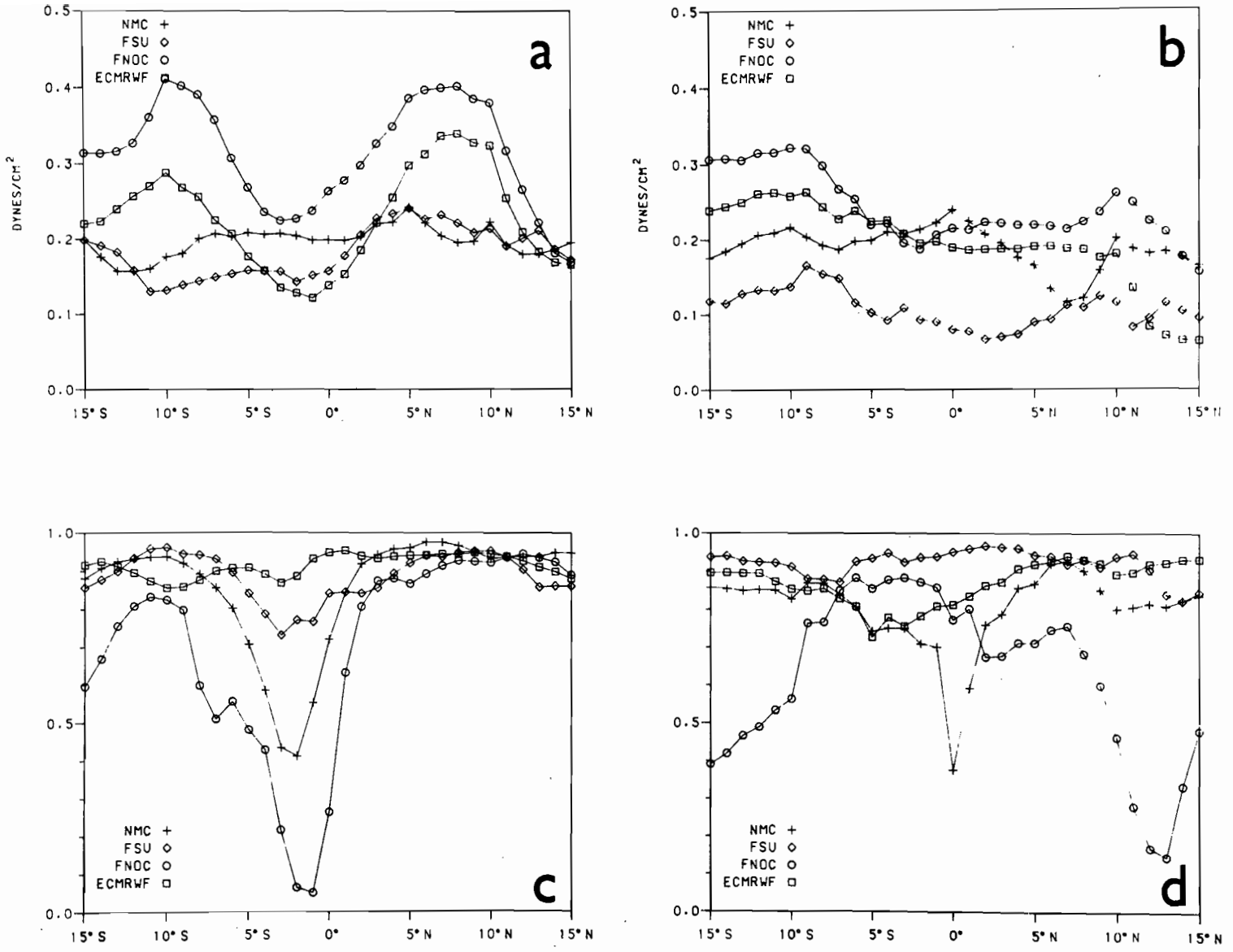

Figure A3: Comparison statistics for zonal and meridional wind stress components on the western Pacific track, comparing the Sadler winds with the four other 1982-83 wind products studied. a) RMS difference in τ^x between the various wind products and the Sadler analysis; b) as (a) except for τ^y; c) correlation of τ^x between the various products and the Sadler analysis; d) as (c) except for τ^y.

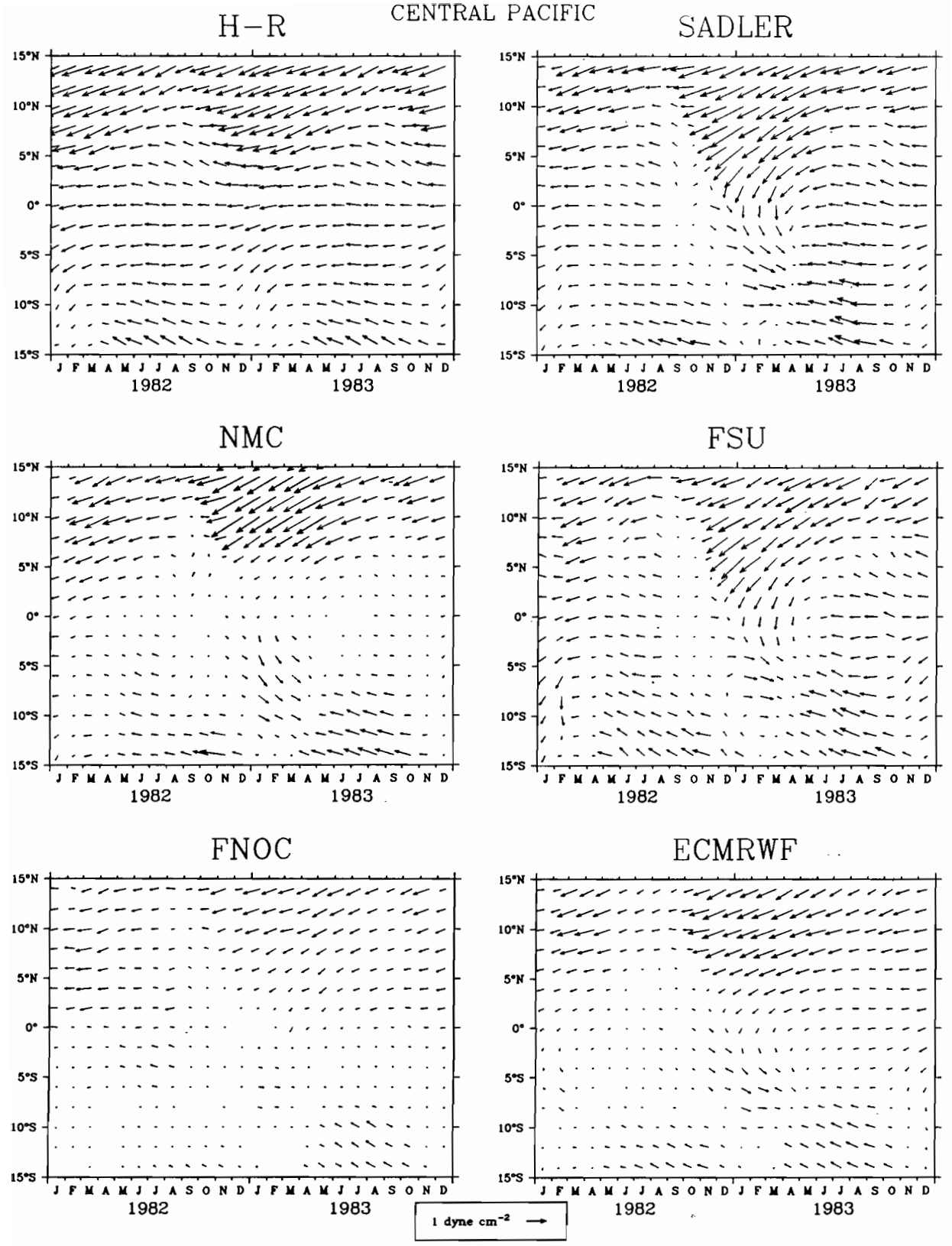

Figure A4: As Figure A1 except for the central Pacific.

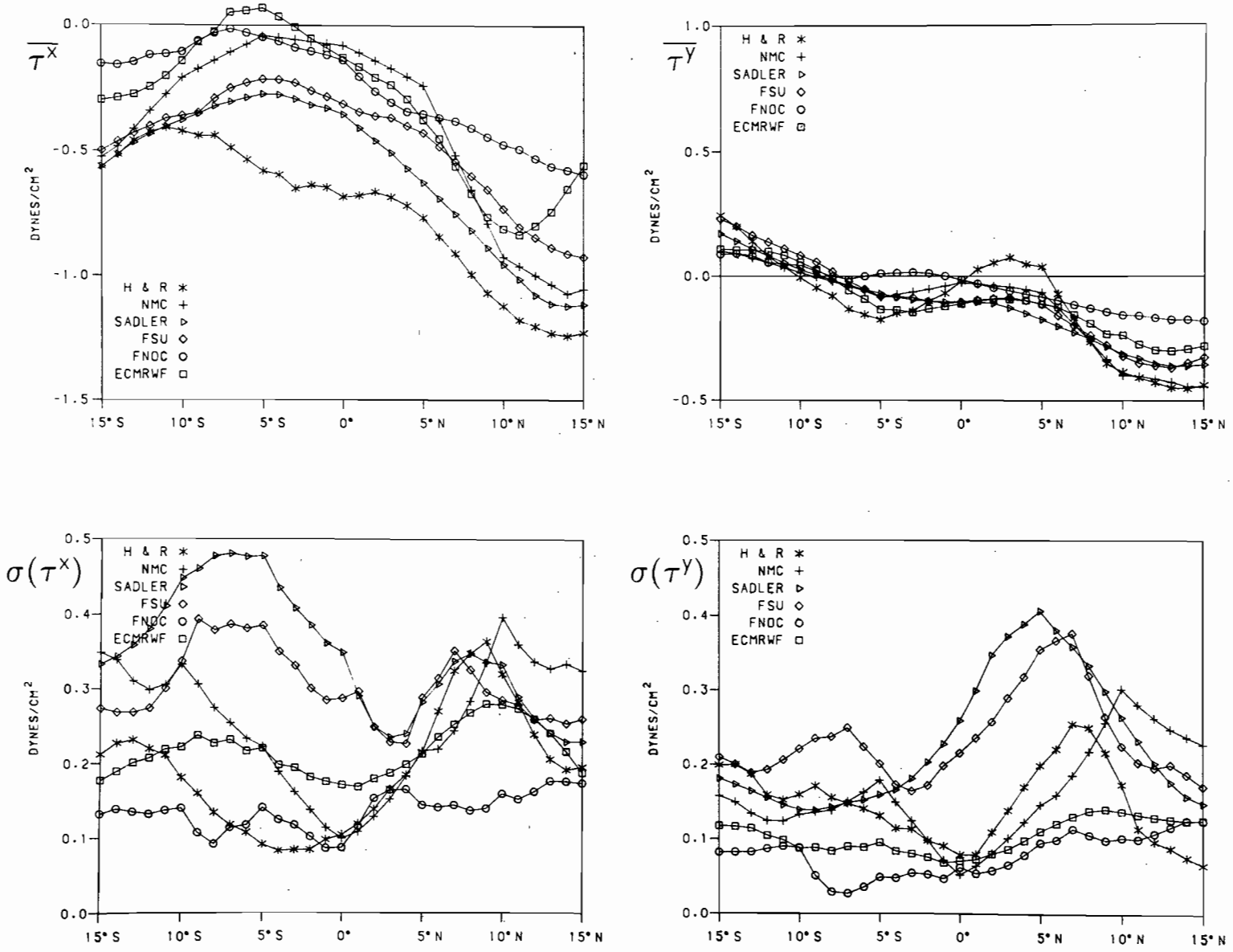

Figure A5: As Figure A2 except for the central Pacific.

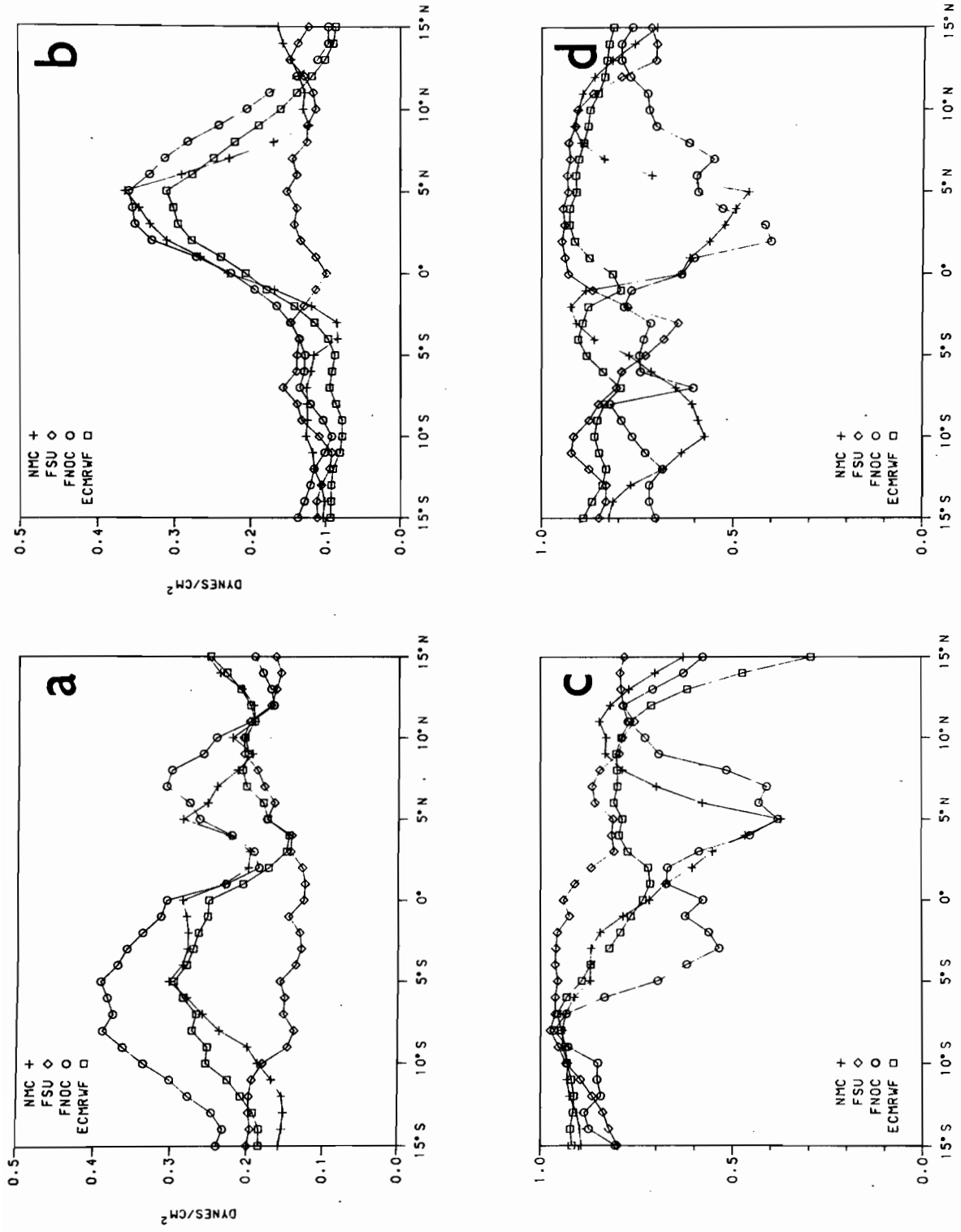

Figure A6: As Figure A3 except for the central Pacific.

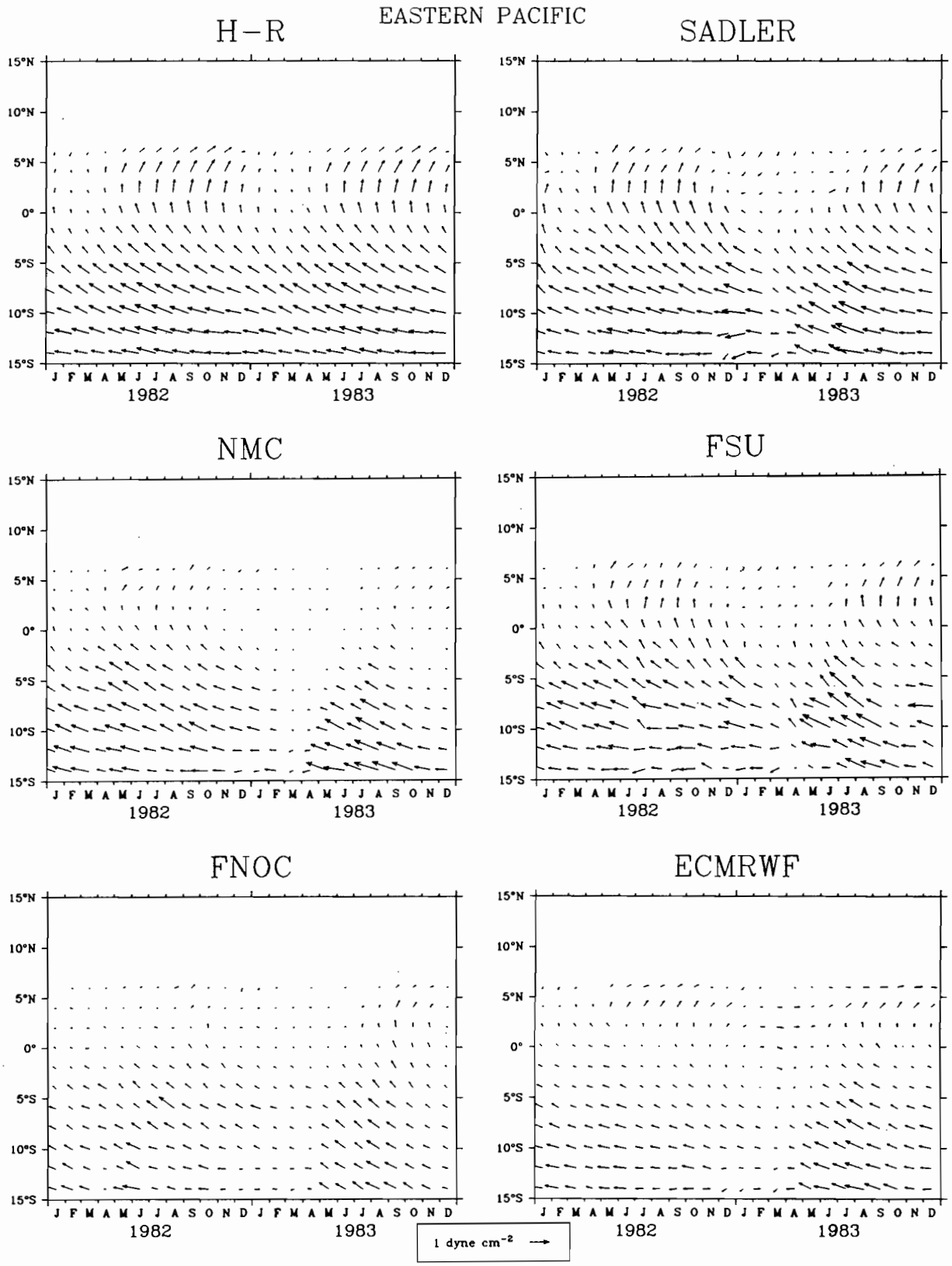

Figure A7: As Figure A1 except for the eastern Pacific.

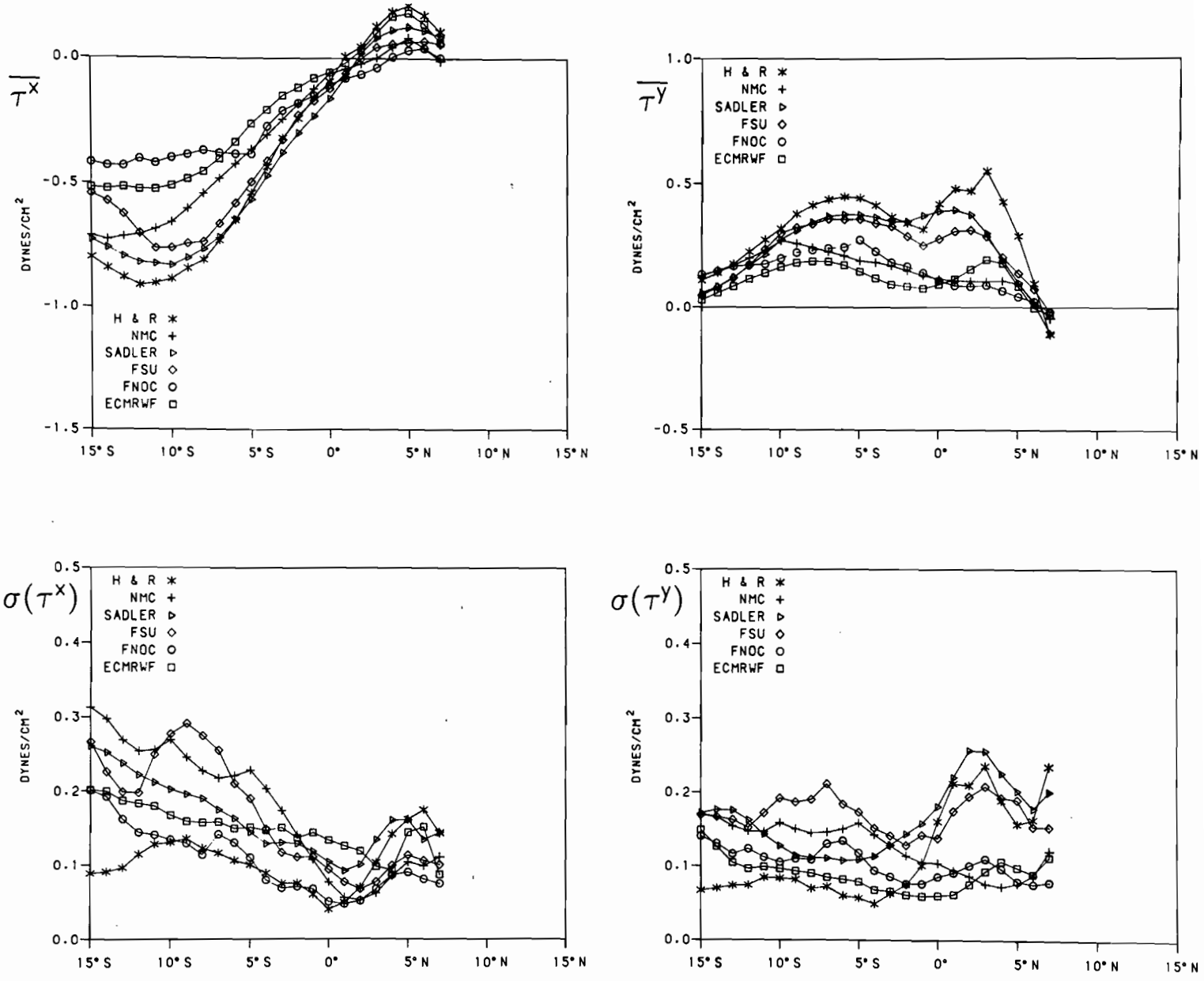

Figure A8: As Figure A2 except for the eastern Pacific.

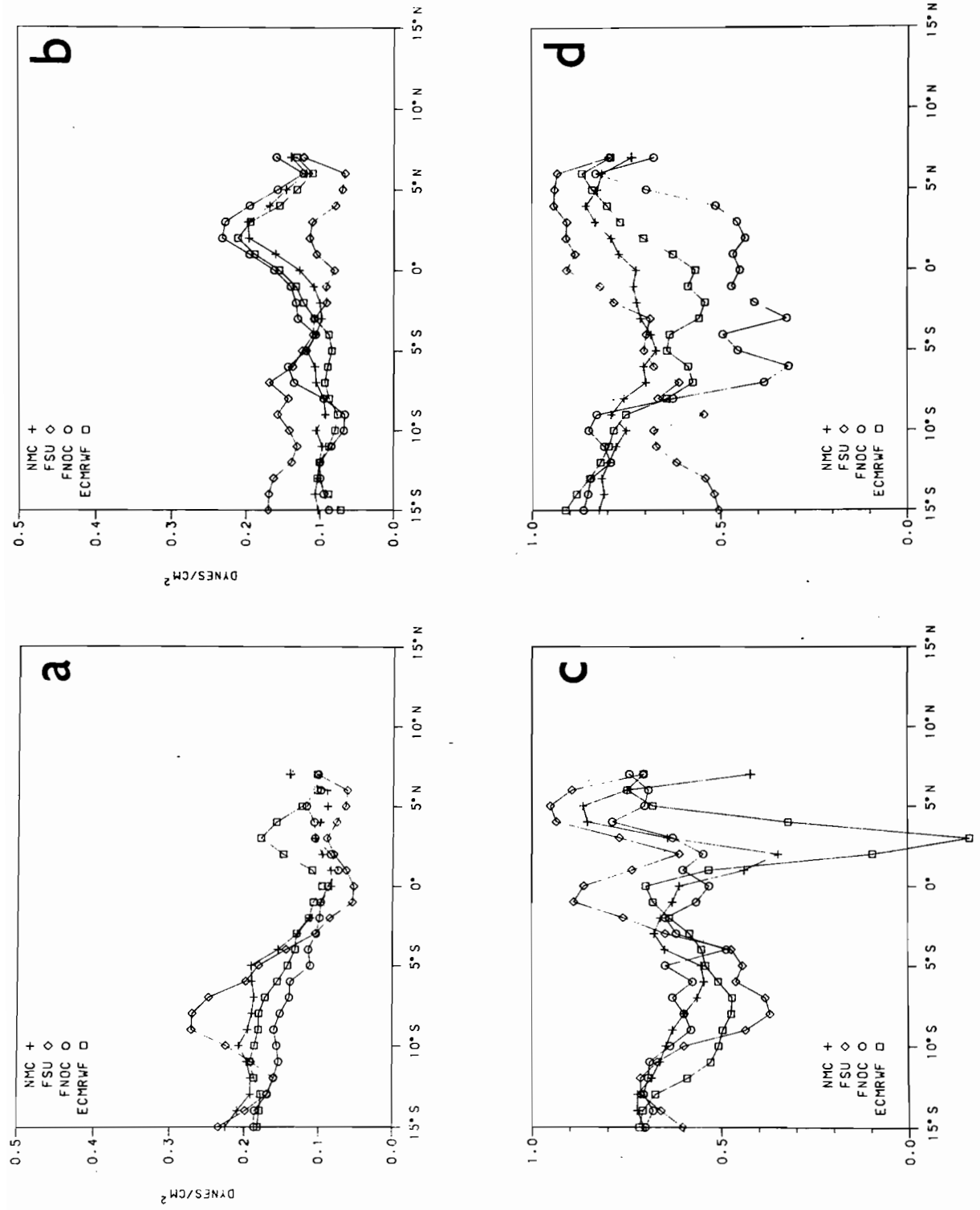

Figure A9: As Figure A3 except for the eastern Pacific.